

Crop Assessment Technique Using a Real-Time Hardware-Based Image Processing System to Support on-the-spot Decision Management for Agricultural Applications

by

Sabiha Shahid Antora

Submitted in partial fulfilment of the requirements
for the degree of Master of Science

at

Dalhousie University
Halifax, Nova Scotia
April 2022

Dalhousie University is located in Mi'kma'ki,
the ancestral and unceded territory of the Mi'kmaq.
We are all Treaty people.

© Copyright by Sabiha Shahid Antora, 2022

DEDICATION

This MSc thesis dissertation is dedicated to my soulmate FM Shoriful Islam, my loving parents, Sarder Shahidul Alam and Luna Arju Lipi, and my caring in-laws' parents Fakir Ashraf Ali and Reshma Begum. Thank you for continually supporting me in my endeavors to better myself and the world around me.

Author

Sabiha Shahid Antora

TABLE OF CONTENTS

LIST OF TABLES	vi
LIST OF FIGURES	vii
ABSTRACT.....	ix
LIST OF ABBREVIATIONS USED.....	x
ACKNOWLEDGEMENTS	xii
CHAPTER 1. INTRODUCTION.....	1
CHAPTER 2. LITERATURE REVIEW	4
2.1 Automation in Agriculture	4
2.2 Image Processing in Agriculture	5
2.3 Real-time Remote Sensing Imagery.....	6
2.4 FPGA-based Image Processing in Agriculture	7
2.5 Georeferencing in Agriculture	9
CHAPTER 3. RESEARCH STATEMENT.....	10
3.1 Research Problem.....	10
3.2 Research Objectives	10
CHAPTER 4. MATERIAL AND METHODS.....	12
4.1 Overview of the Real-time Crop Monitoring System	12
4.2 Real-Time Data Collection Unit	13
4.2.1. RFIP sensing system.....	15
4.2.1.1. Image Acquisition Unit.....	17
4.2.1.2. Image Processing Unit	19
4.2.1.3. Real-Time Data Transfer Unit	21
4.2.2. RTK-GPS System.....	23

4.3 Data Storing Unit	25
4.4 Post-Processing Unit	26
4.5 Performance Analysis and Visualization	27
4.6 Testing of the System	27
4.6.1. Testing of the RFIP System – Lab Environment.....	27
4.6.1.1. Data Collection using the RFIP System	29
4.6.1.2. Acquisition of Reference Data.....	30
4.6.2. Testing of the RFIP System – Outdoor Environment	30
4.6.3. RTK-GPS Accuracy	32
4.6.4. Testing of the Real-time Crop Monitoring System	33
4.7 Performance Evaluation of the System	36
4.7.1. Performance Evaluation of the RFIP System in the Lab and the Outdoor Environment	36
4.7.2. Performance Evaluation of the RFIP System in the Field Environment.....	38
CHAPTER 5. RESULTS AND DISCUSSION.....	40
5.1 Results	40
5.1.1. Experimental Results of Lab Evaluation.....	40
5.1.2. Experimental Results of Outdoor Evaluation.....	45
5.1.3. Visualization of the Data Collected using RTK-GPS	48
5.1.4. Experimental Results of Field Evaluation.....	48
5.2 Discussion	52
CHAPTER 6. CONCLUSIONS.....	54
REFERENCES.....	56
APPENDIX. RAW DATA.....	63
1. RAW Pixel Data from Lab Evaluation	63
2. Example of RAW Image Data from Lab Evaluation	68
3. RAW Pixel Data from Outdoor Evaluation	69

4. Example of RAW Image Data from Outdoor Evaluation	74
5. RAW Pixel Data from Field Evaluation	75
6. Example of RAW Image Data from Field Evaluation	79

LIST OF TABLES

Table 4.1: Switch control logic for the desired output.....	21
Table 4.2: Objects formation with shapes and colors for the performance evaluation of R-ratio, G-ratio, and B-ratio filter.....	29
Table 5.1: Number of pixels detected from the ROI area along with the SD for 16 objects using three-color ratio filters.....	41
Table 5.2: Percentage of deviation for three-color ratio filters.....	42
Table 5.3: Number of pixels detected using the RFIP system and the Web Camera imaging system from the ROI area along with the SD for 22 objects (Romaine lettuce plants).....	45
Table 5.4: Number of pixels detected from the ROI area along with the SD using G-ratio filter.....	49
Table 5.5: Summary of performance analysis.	52

LIST OF FIGURES

Fig. 2.1: Automation in agriculture (variable rate sprayer; Esau et al., 2014).....	4
Fig. 2.2: Potential advantages of using FPGA in remote-sensing data processing (Gonzalez et al., 2011).....	8
Fig. 4.1: Block diagram of the real-time crop monitoring system.....	13
Fig. 4.2: Overview of the required devices, hardware, and connections for the real-time data collection system.	14
Fig. 4.3: FPGA development board, DE2-115.	15
Fig. 4.4: Block diagram of the RFIP system.....	16
Fig. 4.5: FPGA configuration chain using Quartus Prime programmer.	17
Fig. 4.6: Block diagram of the D8M board.....	18
Fig. 4.7: DE2-115 development board connected with D8M camera board.	19
Fig. 4.8: Binary image of the region of interest (ROI) using the color filter and image acquisition hardware.	20
Fig. 4.9: The UART communication channel for real-time data transfer.....	22
Fig. 4.10: The C94-M8P application board with necessary connections.	24
Fig. 4.11: The communication among RTK base station, RTK rover, and the satellites.	25
Fig. 4.12: Data storing PC with necessary connections.....	26
Fig. 5.1: Comparison between pixels detected as red using the RFIP system and the DSLR reference imaging system.	42
Fig. 5.2: Comparison between pixels detected as green using the RFIP system and the DSLR reference imaging system.	43
Fig. 5.3: Comparison between pixels detected as blue using the RFIP system and the DSLR reference imaging system.	43

Fig. 5.4: Correlation between ground truth detected area using the DSLR and actual detected area using the RFIP system (RFIP=1.0327DSLR; $R^2=0.9956$; RMSE=6019.923 Pixels; n=480; $P<0.05$). 44

Fig. 5.5: Comparison between pixels detected as green (the plant leaf area) using the RFIP system and the Web Camera reference imaging system. 46

Fig. 5.6: Correlation between ground truth detected area using the Web Camera and actual detected area using the RFIP system (RFIP=0.8868 Web Camera; $R^2=0.9994$; RMSE=9409.591 Pixels; n=220; $P<0.05$). 47

Fig. 5.7: The GPS data from four spots was recorded and utilized to visually represent the spots which are practically situated in the cm-scale. 48

Fig. 5.8: The geolocations recorded using RTK-GPS with 8 cm accuracy. 49

Fig. 5.9: Comparison between pixels detected as green (the plant leaf area) by the RFIP system and the Web Camera reference imaging system. 50

Fig. 5.10: Correlation between ground truth detected area using the Web Camera and predicted detected area using the RFIP system (RFIP_C=0.9608 Web Camera; $R^2=0.9566$; RMSE=30281.66 Pixels; n=147; $P<0.05$). 51

ABSTRACT

Despite the advances in modern technology, one of the most challenging tasks remains the identification of stressed and/or diseased crops at the field scale. A wide range of precision agriculture (PA) technologies with the integration of remote sensors, Global Positioning System (GPS) and Geographic Information System (GIS), are continuously serving the agriculture industry. Though PA technologies are still evolving, there are some limitations to efficiently apply PA solutions at the field scale, including high computational cost, high complexity, low image resolution, and low GPS accuracy. While Field Programmable Gate Array (FPGA)-based flexible hardware solutions can be a cost-effective and simple alternative to the current multiprocessor systems, it is not widely used in PA. On the other hand, Real-time Kinematic GPS (RTK-GPS) provides the opportunity to achieve cm level accuracy for geographical data collection purposes. Therefore, this study is based on the integration of FPGA-based real-time image processing system, along with highly accurate RTK-GPS data to develop a real-time crop monitoring system. The result is a decision support system that delivers a heat map to the end-users based on the intensity of the detected parameter from the field of interest to assist in site specific farm management solutions. Through this study, the developed system proved its potentiality to resolve some of current PA limitations to provide on-the-spot decisions by combining FPGA-based image acquisition and processing along with high positional accuracy.

Keywords: Real-time, image processing, FPGA, RGB, RS232, and color ratio filter, G-ratio, RTK-GPS, high-resolution, accuracy, heat map.

LIST OF ABBREVIATIONS USED

API - Application Programming Interface

B - Blue

C -Circle

CCC - Concordance Correlation Coefficient

CPU - Central Processing Unit

CSS - Cascading Style Sheets

CSV - Comma Separated Value

D - Diamond

DSLR - Digital Single-Lens Reflex

DSU - Data Storing Unit

FAO - Food and Agriculture Organization

FPGA - Field Programmable Gate Array

G - Green

GIS - Geographic Information System

GLONASS - Globalnaya Navigazionnaya Sputnikovaya Sistema

GNSS - Global Navigation Satellite System

GPIO - General Purpose Input/Output

GPS - Global Positioning System

HTML - Hypertext Markup Language

IC - Integrated Circuits

I²C - Inter-Integrated Circuit

JS - JavaScript

Lab - Laboratory

MIPI - Mobile Industry Processor Interface

O - Oval

OS - Operating System

PA – Precision Agriculture

PC - Personal Computer – PC
PPU - Post-Processing Unit
RTCM - Radio Technical Commission for Maritime Services
R - Red
 R^2 - R-Squared
RA - Rectangle
RDCU - Real-time Data Collection Unit
RFIP - Real-time FPGA-based Image Processing
RMSE - Route Mean Square Error
ROI - Region of Interest
RS232 - Recommended Standard 232
RTK-GPS - Real-Time Kinematic Global Positioning System
RTS - Request to Send
S – Square
SD – Standard Deviation
SDRAM - Synchronous Dynamic Random-Access Memory
SRAM - Static Random-Access Memory
SoC - System on Chip
SOF - SRAM Object File
SWE - Sensor Web Enablement
T - Triangle
UART - Universal Asynchronous Receiver and Transmitter
USB - Universal Serial Bus
VGA - Video Graphics Array
VR - Variable Rate
WVL - Web-based Visualization Layer

ACKNOWLEDGEMENTS

First and foremost, I want to express my gratitude to Almighty Creator for providing me with this wonderful opportunity to complete my graduate study from the Department of Engineering, Faculty of Agriculture, Dalhousie University. I would like to thank my supervisors, Dr. Young Ki Chang, and Dr. Tri Nguyen-Quang, for their professional guidance, encouragement, and persistence during my research project. Thank you for your constructive and productive feedback in every step of my study and work. Analytical abilities and writing skills have considerably been improved by understanding the precision agriculture field through your thoughtful and positive input. I want to express sincere appreciation to my committee members, Dr. Travis Esau, Dr. Ahmad Al-Mallahi, and Dr. Brandon Heung, for their ultimate support. I am thankful for their continuous support and patience throughout my research work and studies.

For the endless guidance and support I received at each stage of my research and to answer any questions I had, I would like to acknowledge the endless support of Dr. Young Ki Chang and Dr. Tri Nguyen-Quang. I would like to express my deepest appreciation to Dr. Young Ki Chang, who has given me the chance to participate in the Lab to Market program for evaluating the research hypothesis of this project in the commercial level. I would also like to acknowledge the helpful and kind support of Dr. Brandon Heung during the statistical analysis for my research project. I want to express my sincere gratitude to MITACS Accelerate program, Lab to Market program and the National Science and Engineering Research Council (NSERC) Discovery Grants Program for the financial assistance they offered to finish this project. I am thankful to Mr. Jason Grant from Dalhousie Agriculture Campus Demonstration Garden for allowing me to use the field for data collection.

The Bio-systems Automation & Robotics Research teams' graduate and internship students, Prabahar Ravichandran, Jaemyung Shin, and Chilin Yu have contributed countless hours to assist me with intuitive input on research project and graduate studies. Muhammad Saad, Anup Kumar Das, and Manoj Natarajan deserve special thanks for their contributions to my project. Thank you Scott Read, metal lab instructor of the Department of Engineering who has worked hard to help me building my data collection framework. Thank you for your immense support.

My acknowledgments would be incomplete if I didn't thank the most substantial source of support, my family. I want to thank my caring husband who helped me for data collection and without his continuous support, I would not be able to finish my graduate study program. I would like to acknowledge the unwavering love and care of my parents, brothers, sisters, and other family members during this journey. In the end, I am deeply obliged to Dr. Young for treating me with immense care and for helping me to acclimatize to Canada. All of this wouldn't be possible without your kind support.

CHAPTER 1. INTRODUCTION

The global population has been increasing, whereby it has grown from 1.65 billion to 6 billion during the 20th century alone (Worldmeters, 2019). The latest report from the Food and Agriculture Organization (FAO) regarding food security and nutrition has shown an increasing trend for the number of people affected by hunger around the world since 2014 (FAO, 2021). Furthermore, based on the Food Insecurity Experience Scale (FIES), there has been an increase of 49.2 million undernourished people from 2014 to 2018, (FAO, 2021).

While global food insecurity is a major concern, there has been a growth in the overall amount of cropland that has been recorded in Canada (Statistics Canada, 2018). Furthermore, traditional methods of cultivation using manual labor has become expensive due to the increased average hourly wage rate for workers in sectors related to natural resources and agriculture (i.e., the average hourly wage rate in Canada for workers in natural resources, agriculture and related production has increased to 32.08% in the last decade; Statistics Canada, 2021). Consequently, the majority of farm operators (55 years and over) in Canada has been using various technologies for their farm operations (Statistics Canada, 2017). In addition, the proportion of farms in Canada using computers and/or laptops for farm management has also increased (Statistics Canada, 2018).

Feeding the rising population has become a challenge for the crop industry; yet the global agricultural employment has reduced from 44% to 28% during 1991 to 2019 (Worldbank, 2019). This indicates the need for precision agriculture (PA) technologies, such as Global Positioning System (GPS), Geographic Information System (GIS), miniaturized computing, advanced information processing, and telecommunications to facilitate reduced agricultural inputs, higher

resource efficiency, and sustainable agricultural management using digital technologies (Zhang et al., 2002). Sustainable crop production intensification has been providing a great support for the crop production optimization per unit area (FAO, 2021). For instance, the Integrated Weed Management (IWM) techniques have applied a diverse suite of weed control methods, such as grazing, herbicide application, land fallowing, and biological control, to reduce crop losses due to weeds (FAO, 2021).

Technological innovation in the agriculture sector have included agricultural robots or ‘agrobots’ (Valle, 2020). This technology can be equipped with automated, variable rate (VR) sprayers with the integration of controllers, computer systems, and remote sensing devices, such as ultrasonic sensors and mounted cameras for the site-specific application of agrochemicals in wild blueberry fields (Esau et al., 2014). The agriculture sector is currently being served by PA and remote sensing technologies to support weed mapping, vegetation growth monitoring, crop health assessments, irrigation management, yield estimation, and crop spraying by offering easy, fast, and cost-effective solutions (Tsouros et al., 2019). However, imagery has been the most common part of these PA technologies, whereby Esau et al. (2014) used digital color cameras to determine plant leaf areas for spot application of fungicide; Rehman et al. (2018) developed an image acquisition Graphical User Interface (GUI) system to control the spray nozzles of a VR sprayer for agrochemical savings during spot application; and Dorj et al. (2017) used digital color camera to detect orange color for yield estimation in citrus orchards.

Farmers need faster processing and real-time actionable information about their field analyses (Myers, 2020). For this reason, they require a feasible PA imaging technology to ensure the optimal use of their agricultural inputs for maximum crop growth while minimizing money

and time (Ling & Bextine, 2017). Processing speed and cost-effectiveness may be some of the major obstacles for current PA image processing techniques to be applied in real-time at the field-scale (Burgos-Artizzu et al., 2011).

As a part of current reconfigurable computing technology, field programmable gate array (FPGA) is an ideal approach for image processing applications (Ramirez-Cortes et al., 2013) with its high processing speed, inherent parallelism of running multiple tasks simultaneously, and cost-effectivity (Ramirez-Cortes et al., 2013; Johnston et al., 2004; AlAli et al., 2014; Price et al., 2006; Zhai et al., 2011). Therefore, the main goal of this study is to address the current PA limitations of computational complexity and develop cost-effective efficient solutions for field-scale farm management applications.

The remainder of this thesis is organized as to discuss about the literature review of current image processing trends in PA including FPGA in chapter 2. Chapter 3 mentions the research objectives and Chapter 4 describes the materials and methods of this study including the experimental test setup. The outcome of the developed system and the test results are described in chapter 5 along with the necessary discussion. The last chapter of this dissertation is the summary of this research as a conclusion.

CHAPTER 2. LITERATURE REVIEW

2.1 Automation in Agriculture

The agricultural sector has been increasingly challenged to feed the rising population, where there is a clear need for the optimization and sustainable intensification of global crop production (FAO, 2021). However, the conventional means of agriculture rely upon manual labor, which is not only physically intensive (Statistics Canada, 2018), but also expensive (Statistics Canada, 2021) to carry out. During this digital era, agriculture has continued to evolve toward the use of data-driven technologies, often involving the use of GPS, GIS, and PA to inform seeding and harvesting practices, as well as the application of agricultural inputs (Statistics Canada, 2017).



Fig. 2.1: Automation in agriculture (variable rate sprayer; Esau et al., 2014).

PA constitutes a suite technology that can capture and analyze field data to inform the targeted management of farms while increasing cost-efficiency and productivity and minimizing environmental impacts (Tsouros et al., 2019). For example, the real-time and site-specific management of the cultivated lands can lead to productivity growth by using PA technologies for

the targeted application of agrochemicals at optimal frequencies and amounts (Tsouros et al., 2019). Among the evolution of various technologies for agricultural automation, image processing is a tremendous inclusion to understanding the insights of the field parameters.

2.2 Image Processing in Agriculture

One important area of research in PA involves digital image analyses, which provides the means to detect, recognize, and describe objects to support management decisions (Schellberg et al., 2008). These image processing techniques are often based on the color, shape, and geometric features of target objects (Saxena & Armstrong, 2014; Vibhute & Bodhe, 2012). Depending on the need to acquire real-time farm data, the techniques for digital image analyses may be used in applications, such as crop row detection, canopy measurement, weed detection, fruit sorting and grading (Saxena & Armstrong, 2014; Vibhute & Bodhe, 2012). Digital image analyses also play an important role for monitoring the plant growth and fruit defects, and the measurement of vegetative indices (Saxena & Armstrong, 2014; Vibhute & Bodhe, 2012).

The use of image processing techniques might be incompatible for some real-time field applications due to the limitations caused by computational time (Burgos-Artizzu et al., 2011) that leads to the urgency for local processing during the collection of images (Saddik et al., 2021). For example, based on color, shapes, and texture analyses, the discrimination of crops and weeds may be computationally complex and unsuitable for real-time field applications (Burgos-Artizzu et al., 2011; Saddik et al., 2021). Despite the fact that image processing is a significant technology for crop monitoring purposes, the analytical incompetence of this technique becomes a tough part for real-time remote sensing purposes (Saddik et al., 2021).

2.3 Real-time Remote Sensing Imagery

Through managing, analyzing, and processing a large amount of farmland data, PA has been providing farm management services to help farmers in decision-making (Zhang, 2016). These services have included the delineation of management zones for VR operations and crop health monitoring (Zhang, 2016). With the help of real-time remote sensing imagery (though the primary idea of this research was the development of an image processing technique to mitigate the analytical incompetence of real-time remote sensing imagery, due to time limitation, the developed technique has been tested using a ground-based monitoring system rather than aerial monitoring system), crop health monitoring has been assisting in identifying the affected crop areas due to insects, weeds, fungal infestations, or weather-related damage (Al-Gaadi et al., 2016; Statistics Canada, 2015). Here, remote sensing imagery, often serves as a source of data to support PA (Zhang, 2016). To provide PA farm management solutions to the farmers, not only the spatiotemporal data collection, but also the data processing, analysis, management, and storage are important (Zhang, 2002).

To generate quantitative PA mapping products, geometric and spectral processing are often applied on the remote sensing imagery (Guo et al., 2012). Guo et al. (2012) found that the crop growth status can be monitored by following the vegetation indices along with the state-of-art GPS location information from the crop stress maps. In addition, the real-time remote sensing data can lead to improved decision-making in PA if high spatial and spectral resolution data are used (Mulla, 2013). Therefore, Real-time control over the farmlands has been maintained using the latest high-performance multiprocessor data computing systems, such as clusters of networks of central processing units (CPUs; Caballero et al., 2020). However, the time gap between data

acquisition and crop information distribution, has become a critical factor for real-time crop management or damage prevention (Statistics Canada, 2015).

To address this limitation, a study proved that FPGA-based, on-chip systems can respond to the real-time constraints of a monitoring system by providing high resolution, consuming less energy, improving processing time, and the number of images processed per second compared to the conventional CPU/GPU-based systems (Saddik et al., 2021). For instance, Kestur et al. (2010) tested the performance and energy efficiency of the FPGA, CPU, and GPU based on the basic linear algebra subroutines, where FPGAs offer comparable performance as well as 2.7 to 293 times better energy efficiency among all three platforms. Hence, FPGAs are an easier alternative to these multiprocessor systems for real-time onboard processing of remotely sensed data (Gonzalez et al., 2011), that has not been applied on the crop monitoring purposes yet. Therefore, to fill the gap between the computational efficiency of remote sensing imagery and real-time crop management, this study focuses on the integration of FPGA-based image processing in agricultural crop monitoring purposes using remote sensing.

2.4 FPGA-based Image Processing in Agriculture

An FPGA is composed of multiple logic blocks connected with programmable interconnect that allows users to implement multi-level logics (Trimberger, 1994). On-board, processing systems, based on FPGAs are reconfigurable, low-cost, and lightweight, which might be used for real-time object identification and tracking (Ramirez-Cortes et al., 2013; Johnston et al., 2004; MacLean, 2005; Bannister et al., 2005; Price et al., 2006). FPGAs are flexible, whereas a wide range of devices are integrated together to reduce the amount of hardware and increase the cost-effectiveness of the system (MacLean, 2005). Furthermore, FPGAs are also described as

reconfigurable hardware because the same device can be reused by downloading a new program for different purposes (Ramirez-Cortes et al., 2013). FPGAs only require hours to carry out the design-implement-test-debug cycle; in comparison, application-specific integrated circuit designs require days to complete all the processing (MacLean, 2005; Bannister et al., 2005). This also has the ability to implement parallel processing that ensures simultaneous multiple local operations, which is necessary for image processing techniques (MacLean, 2005; Price et al., 2006).

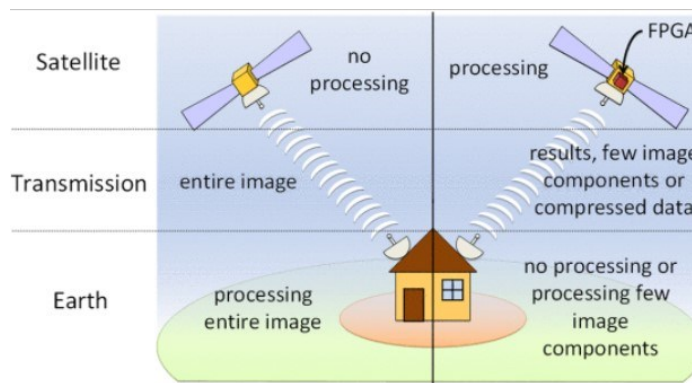


Fig. 2.2: Potential advantages of using FPGA in remote-sensing data processing (Gonzalez et al., 2011).

FPGA implementations do not have widespread acceptance in the image processing community yet (MacLean, 2005; Seagusa et al., 2008; Asano et al., 2009; Tlelo-Cuautle et al., 2015), although a few studies have been done on unmanned aerial vehicle-based cars and land vehicles identification (Moshnyaga et al., 2008). FPGAs have also been used for real-time, license plate localization (Zhai et al., 2011) and human presence detection systems (Moshnyaga et al., 2008). Though FPGAs have been used in remote sensing (Gonzalez et al., 2011; El-Medany & El-Sabry, 2008; González et al., 2013), it has not been applied for agricultural applications specifically. However, for image processing purposes, FPGAs have been tested on a wide range of low-resolution dimensions; for example, 180×180 pixels to 600×600 pixels (Price et al., 2006); 128×128 pixels (Ramirez-Cortes et al., 2013); 256×256 pixels (Bannister et al., 2005);

640 × 480 pixels (Cointault et al., 2012; Zhai et al., 2011); and 816 × 600 pixels (Dou et al., 2019), while it has the potential to be applicable for high-resolution dimensions. Hence, the development of real-time image acquisition and processing system based on FPGA hardware for crop monitoring purposes is one of the two major focuses of this research. Another major focus of this research is the integration of GPS technology with high positional accuracy, as this is another significant part of crop monitoring (Guo et al., 2012).

2.5 Georeferencing in Agriculture

GPS and GIS technologies have been integrated with the remote sensing technique to determine long-term farm management decisions, such as assessment of tillage systems (Sood et al., 2015). For this purpose, comprehensive, georeferenced, real-time, or almost real-time data have been the predominant building blocks (Sood et al., 2015). Hence, a farmer may quickly locate the problematic area in his field by following the georeferenced data (Statistics Canada, 2015).

For site-specific crop management decisions, Rub and Brenning (2010) established the spatial relationships between geographical data, soil parameters, and crop properties. However, georeferencing using a GPS with a positional accuracy of <1 m is needed for monitoring plant canopy status, yield mapping, weed mapping, and weed detection techniques to construct the most accurate map in VR PA applications (Lamb & Brown, 2001; Zude-Sasse et al., 2016). To address this issue, real-time kinematic (RTK)-GPS may achieve a few cm-scale positional accuracy, whereby Sun et al. (2010) proved its feasibility through automatically mapping the transplanted row crops. Henceforth, to fill the gap of high positional accuracy requirement for crop monitoring purposes, this study includes the integration of RTK-GPS along with the FPGA-based real-time image acquisition and processing for the basis of real-time crop monitoring.

CHAPTER 3. RESEARCH STATEMENT

3.1 Research Problem

From the literature review of current image processing techniques in PA, it was found that processing images on-board while collecting images has some computational limitations (Burgos-Artizzu et al., 2011; Sddik et al., 2021; Bhakta et al., 2019). Whereas FPGA hardware provides the flexibility to perform both operations on a single processor (Moshnyaga et al., 2008; Zhai et al., 2011), it has not been tested for the agricultural crop monitoring applications yet (Gonzalez et al., 2011; El-Medany & El-Sabry, 2008; González et al., 2013). Consequently, the application of PA farm management solutions in practical field requires more accurate GPS data (i.e., a few centimeters positional accuracy) to construct the most accurate map (Lamb & Brown, 2001).

3.2 Research Objectives

Therefore, this study proposes a computationally efficient and cost-effective real-time crop monitoring system which includes a real-time FPGA-based image processing system that is RFIP with high resolution imagery and an RTK-GPS with a few cm positional accuracy. The specific objectives of this study are listed below:

- (1) to develop a high-resolution RFIP system;
- (2) to develop a system for transferring the processed image data in real-time;

- (3) to develop the real-time crop monitoring system that includes an RFIP and an RTK-GPS to identify plant leaf areas in a Romaine lettuce (*Lactuca sativa* L. var. *longifolia*) crop field;
- (4) to develop a real-time data collection and post-processing system to find the pixel area detected as plant leaf areas;
- (5) to evaluate the performance of the real-time crop monitoring system in lab, outdoor, and field environment.

The research hypothesis of this study are: if the real-time image processing system is developed using the reconfigurable and parallel FPGA hardware, the crop monitoring will be computationally competent; as well as, if the RTK-GPS with a few cm positioning accuracy is added with the real-time image processing, the crop monitoring system will be able to provide the most accurate map of the field including crop assessment results.

CHAPTER 4. MATERIAL AND METHODS

To summarize the methods of this study, image acquisition was performed using a mobile industry processor interface (MIPI)-based D8M camera board (Terasic Inc.; Hsinchu City, Taiwan), with a resolution of 800×600 pixels. The captured imagery was processed using a DE2-115 FPGA development board from the Altera Cyclone IV FPGA family (Intel Inc.; Santa Clara, California, USA). Real-time processing utilized various module blocks of the Altera Cyclone IV processor, which applied three different color ratio filters, and a threshold filter. The processed data consisted of the number of pixels detected, whereby the detected pixel area was transferred to another computing device, in real-time, by following a serial communication protocol. The performance of the proposed system was evaluated both in the lab, outdoor, and field environment, where the real-time data was compared with manually processed images of the same target, captured by a digital single-lens reflex (DSLR) camera, as a reference for the lab environment, and a web camera, as a reference for the outdoor and field environment. Also, Google Earth Pro software (Google Inc.; Mountain View, California, United States) was used to visualize the performance of the RTK-GPS.

4.1 Overview of the Real-time Crop Monitoring System

The overall functionality of the real-time crop monitoring system is depicted in Fig. 4.1. Firstly, the RFIP system is developed with a DE2-115 FPGA board and a D8M camera board to acquire and process the real-time images. An RTK high accuracy solution from the u-blox NEO-M8P-2 module, C94-M8P application board, (u-blox Inc.; Thalwil, Switzerland) is configured for an 8 cm accuracy. The RFIP and RTK-GPS are the real-time data collection devices that are

combined and referred to as the real-time data collection unit (RDCU) in this study. The data collection units were maintained to record data from a ground height of 3.5 ft to 4 ft. One of the principal goals of this study was to test the system on a robotic vehicle but due to time limitation the RDCU was developed to collect data in a standstill position. Here, one personal computer (PC), connected with the output ports of the RDCU, serves as a data storing unit (DSU). The Python programming Tool (Python Software Foundation Inc.; Wilmington, Delaware, USA) is installed in the DSU to read the RDCU output ports and geotag the real-time field data using the AVERMEDIA Live Streamer CAM 313 (AVerMedia Inc.; New Taipei City, Taiwan) web camera reference images. To analysis the performance of the RFIP system and visualize the real-time field data, the collected real-time georeferenced images are fed to the post-processing unit (PPU). The PPU consists of the same PC and programming language as DSU, but the processing does not require real-time data acquisition.

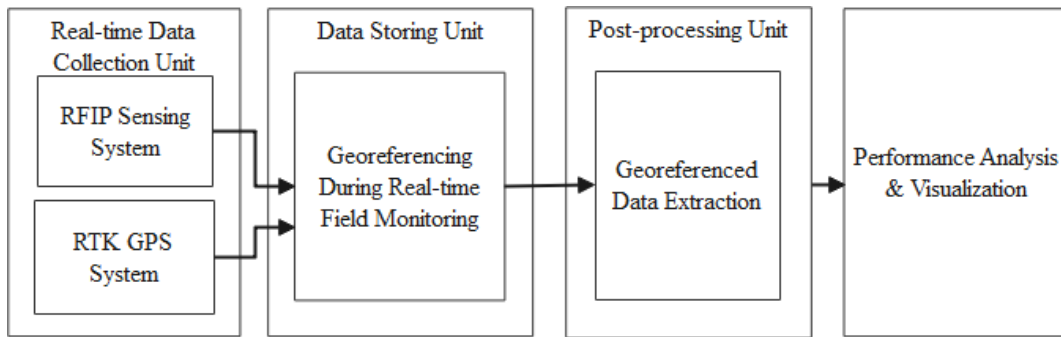


Fig. 4.1: Block diagram of the real-time crop monitoring system.

4.2 Real-Time Data Collection Unit

One of the major components of this research is the RDCU, which is the prototype of an agile, real-time, FPGA-based, and lightweight data collection system. For development and testing purposes, the necessary hardware and devices are installed on a horizontal T-shaped wooden frame. After installation, the custom-built wooden frame is attached with metal and screw on top

of a tripod that has adjustable legs which can be extended to 5 feet in length, as well as rotatable in left or right directions.

The tripod set up includes the following (Fig. 4.2): (1) one of two identical RTK boards, which is configured as rover having two antennas global navigation satellite system (GNSS) and UHF; (2) the RFIP system consisted of the FPGA board, and D8M camera board to acquire and process images; and transfer detected pixel area in real-time; (3) one liquid crystal display (LCD) monitor that is connected to the VGA output port of the FPGA development board to display the output images following some switching logics; (4) a web camera to geotag the GPS location and the detected pixel area; (5) a battery source with a 400 W power inverter to supply power to the FPGA device and the LCD monitor; (6) one PC to supply power to the USB web camera, to supply power to the RTK rover, and to download the Quartus Prime (Intel Inc.; Santa Clara, California, USA) program configuration file to the FPGA board, which is connected to the RS232 serial output port of RFIP system; and (7) one blue painted wooden frame having an area of 30×22.5 cm to maintain a consistent camera projection at a fixed ground resolution over the selected spots.

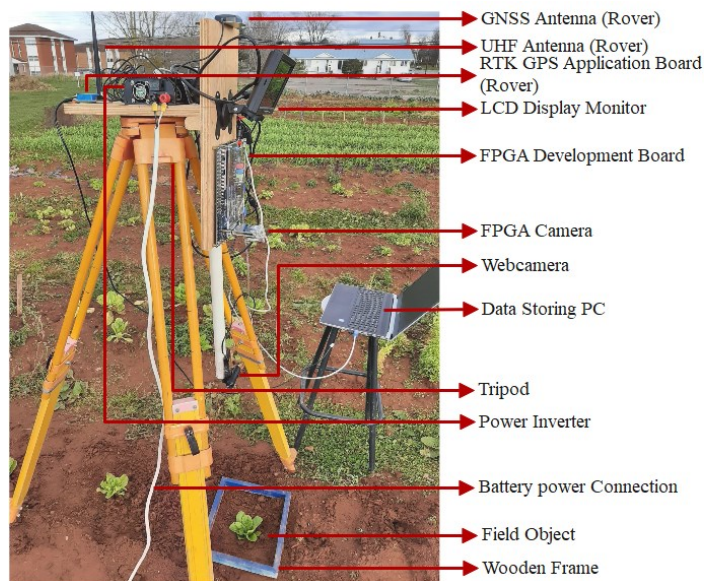


Fig. 4.2: Overview of the required devices, hardware, and connections for the real-time data collection system.

4.2.1. RFIP sensing system

The Altera Cyclone IV 4CE115 FPGA device, DE2-115 development board was chosen as the main controller of the RFIP system (Fig. 4.3). It has a universal serial bus (USB) blaster (onboard) port to download programs for specific applications. Furthermore, a part of the 2MB static random-access memory (SRAM) and 128MB synchronous dynamic random-access memory (SDRAM) memory buffers was used primarily to store the camera sensor outputs that needed to be processed. In addition, a few pushbuttons and slide switches were used to control the algorithms for image processing. To display the processed image, video graphics array (VGA) and 8-bit high-speed triple digital to analog converter integrated circuits (ICs) with VGA-out connector were used as output pipelines. A Recommended Standard 232 (RS232) transceiver IC with a 9-pin connector and flow control were used to transfer the detected pixel area in real-time. Another important component of the DE2-115 development board was a 40-pin expansion header with diode protection and a General-Purpose Input/Output (GPIO) interface to communicate with the camera board.

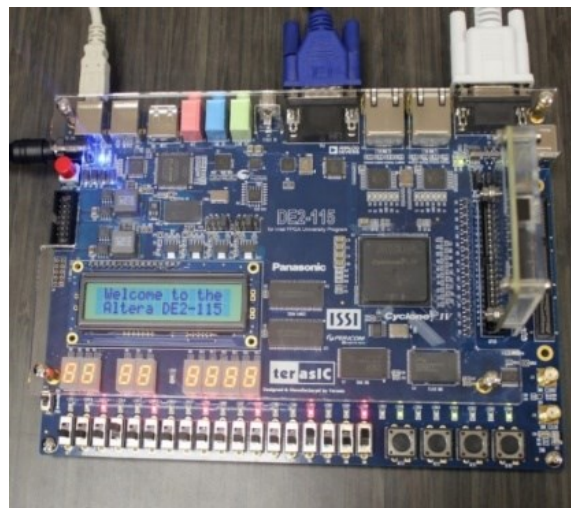


Fig. 4.3: FPGA development board, DE2-115.

The overall functionality of this RFIP system is depicted in Fig. 4.4. Firstly, the system is acquiring the real-time camera sensor input by using look-up tables. Following this, the 10-bit serial image stream is written to the SDRAM memory buffer and read using an application-specific image resolution mask. The read image frame from the memory buffer is then buffered again using horizontal and vertical control signals in the SRAM line buffer. Next, a high-level control signal is used to convert the raw 10-bit image data from the line buffer into a 24-bit RGB image. To read pixels of the image frame, The control signal depends on the VGA clock, vertical synchronization signal, and read request control signal generated from the VGA controller system.

The image processing unit utilized the 24-bit RGB images and processes them in two steps by using the R/G/B ratio filter and the thresholding filter. As the image processing system uses three different basic color detection algorithms (R-ratio, G-ratio, and B-ratio filters), a switching logic was developed with the combination of four switches from the development board to provide four different output images. Finally, the processing unit provides two different outputs: the original or binary images on the VGA monitor; and the number of pixels, detected as red, green, or blue, to the external computing device for data analyses.

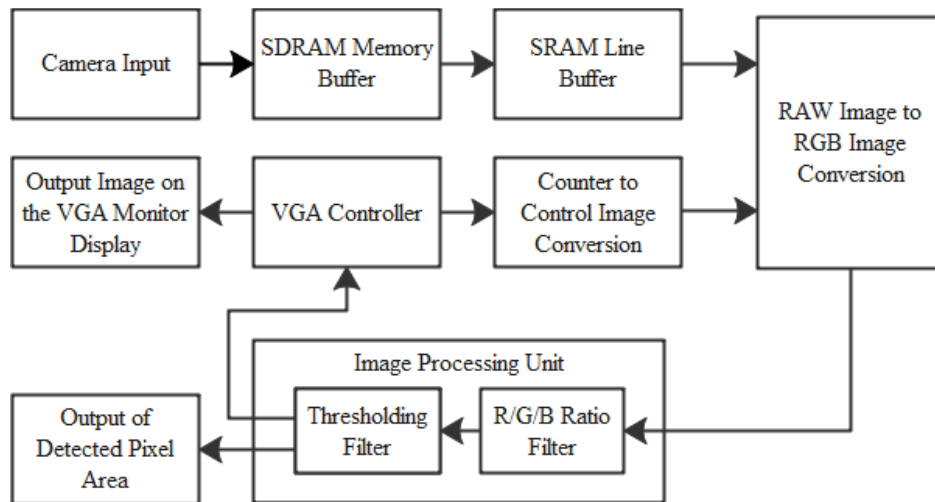


Fig. 4.4: Block diagram of the RFIP system.

The software packages used to design, program, and extract the image data were needed for developing the RFIP system (Fig. 4.5). Once a design was completed, the Quartus Prime (Intel Inc.; Santa Clara, California, USA) software was used to generate an SRAM object file (SOF) in a file directory. The SOF contains the data for configuring all SRAM-based, Altera devices, supported by the Quartus Prime software. The USB blaster circuitry provided the program download interface to the Altera device's processor using a Type A-B USB cable. Finally, the FPGA hardware was configured to the developed design by using the Programmer Tool.



Fig. 4.5: FPGA configuration chain using Quartus Prime programmer.

4.2.1.1. Image Acquisition Unit

The image acquisition hardware consisted of an 8-megapixel digital camera development package (Fig. 4.6), D8M, which included a MIPI camera module and a MIPI decoder that provided 10-Bit parallel Bayer pattern image data. The MIPI camera module outputs 4 lanes of MIPI interface image data, which can be converted to parallel data by passing through the MIPI decoder IC to the GPIO interface. The D8M board was connected to the DE2-115 FPGA development board via a 2×20 GPIO pin connector. Both the MIPI camera module and MIPI decoder of the D8M camera were controlled by the FPGA using an inter-integrated circuit (I²C) communication protocol.

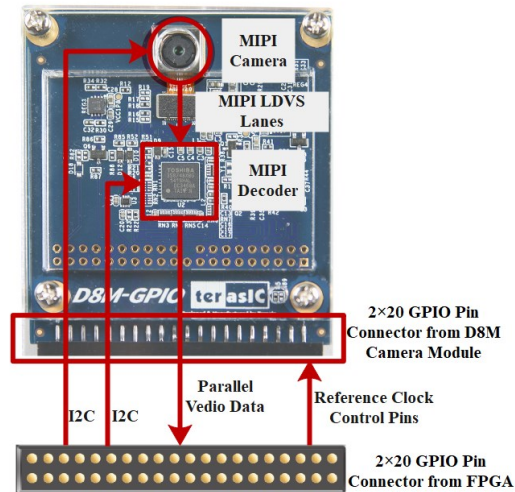


Fig. 4.6: Block diagram of the D8M board.

The D8M board was equipped with an 8-megapixel MIPI image sensor, OV8865, with a lens size of 1/3.2" and pixel size of $1.4 \mu\text{m} \times 1.4 \mu\text{m}$ (OmniVision Inc.; Santa Clara, California, USA). The OV8865 sensor acquired image at a 3264×2448 pixels resolution, at 30 frames per second, with a 70° view angle. It should be noted that the sensor has additional flexibility in acquiring imagery at multiple resolutions using windowing and cropping functions, while maintaining the corresponding field of view.

For programming the real-time image acquisition unit, the Verilog programming language was used in the Quartus Prime Lite 18.0 software tool. To change the output image resolutions, the OV8865 needed to be configured via I²C so the camera could output the desired image format. Furthermore, the analog gain, digital gain (i.e., red, green, and blue channel gain), and exposure gain were chosen by several experiments and adjustments for the required 800×600 pixels resolution. The required clock frequency needed for the acquisition of the imagery was determined by adjusting the parameters from the Quartus Prime's IP resources. For this study, an output clock of 40MHz was used to achieve the acquisition of 800×600 pixels resolution imagery at 40 frames per second.

4.2.1.2. Image Processing Unit

The hardware for image processing consisted of the DE2-115 development board. No additional hardware was used for the processing except for the image processing filter pipeline between the raw image to RGB converter and the VGA display controller. The raw image to RGB converter receives 10-bit raw image data output from the D8M camera board and converts that into 24-bit RGB images.

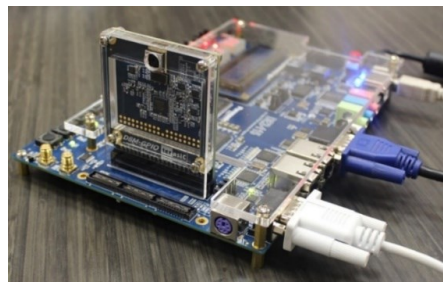


Fig. 4.7: DE2-115 development board connected with D8M camera board.

After establishing the communication between the D8M camera board and the DE2-115 FPGA board (Fig. 4.7), the raw image data is converted to RGB image data, consisting of three different color components: red (R), green (G), and blue (B). Using high-level, logic control derived from the VGA display controller module. These three-color components are used to display the original RGB image of the object, which is placed in front of the D8M camera board, on the VGA display monitor. The image processing unit inputs the 24-bit RGB image data (i.e., 8-bit R component, 8-bit G component, an 8-bit B component of the color image) and applies the color ratio filter (i.e., R-ratio, G-ratio, or B-ratio filter) followed by threshold filter on the R, G, and B color components. However, one out of four processing operations: original RGB image; binary image of red objects; binary image of green objects; and binary image of blue objects, can be performed at a time by following the developed switching logic. A sample of the original object, its original RGB image, and the detected binary image is shown in Fig. 4.8.

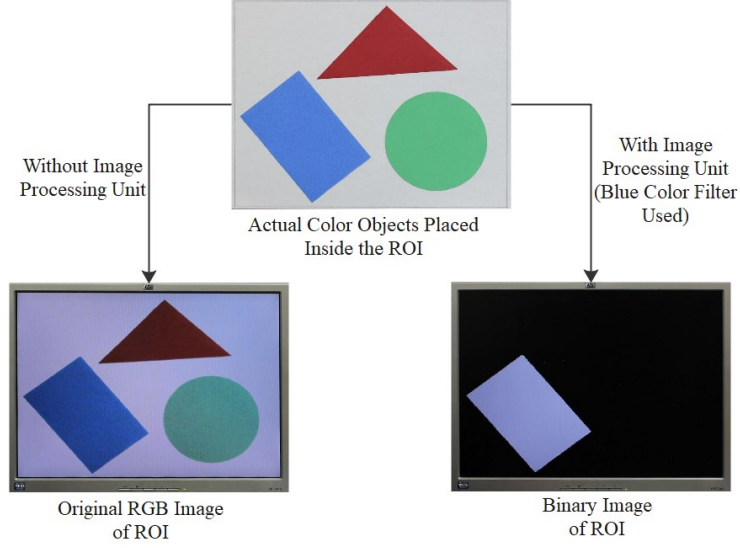


Fig. 4.8: Binary image of the region of interest (ROI) using the color filter and image acquisition hardware.

Previous studies have used the G-ratio formula: $(255 \times G) / (R + G + B)$ for 24-bit RGB image analysis from wild blueberry fields for spot-application of granular fertilizer (Chattha et al., 2014). Therefore, the formula was modified to perform R-ratio and B-ratio filter analysis as follows: $(255 \times R) / (R + G + B)$ and $(255 \times B) / (R + G + B)$, respectively. A threshold of intensity 90 was selected for each of the color ratio filters to produce the binary image with the detected area as white by setting the processed R, G, and B output color components (R_o , B_o , and G_o) at the maximum intensity, 255. Lastly, the final formulas for the real-time image processing unit for the three-color detection techniques are shown in Eqs. 1-3:

$$R - ratio: \text{If } R > 0 \ \& \ \frac{255 \times R}{R + G + B} > 90, \ R_o, \ B_o, \ \text{and } G_o = 255, \ \text{otherwise } 0 \quad (\text{Eq. 1})$$

$$G - ratio: \text{If } G > 0 \ \& \ \frac{255 \times G}{R + G + B} > 90, \ R_o, \ B_o, \ \text{and } G_o = 255, \ \text{otherwise } 0 \quad (\text{Eq. 2})$$

$$B - ratio: \text{If } B > 0 \ \& \ \frac{255 \times B}{R + G + B} > 90, \ R_o, \ B_o, \ \text{and } G_o = 255, \ \text{otherwise } 0 \quad (\text{Eq. 3})$$

The developed switching logic uses four switches to select one image processing operation among four (Table 4.1). For displaying the original RGB image of the ROI, all four switches are set to low. To select any of the R, G, and B color detection techniques, switch 3 and one of the corresponding switches 0, 1, or 2 should be set to high.

Table 4.1: Switch control logic for the desired output.

Index	Switch3	Switch0	Switch1	Switch2	Filtered Output
1	0	0	0	0	Original Color Image
2	1	1	0	0	Detected Binary Image of Red Object
3	1	0	1	0	Detected Binary Image of Green Object
4	1	0	0	1	Detected Binary Image of Blue Object

4.2.1.3. Real-Time Data Transfer Unit

The number of pixels detected as R, G, or B, determined from their respective color ratio filters was needed to be determined from the system. Each time a pixel from an image frame satisfies the specified color detection formula (Eqs. 1-3), the corresponding pixel is modified from a color pixel to a white pixel and counted as a detected pixel inside the ROI. When a pixel does not satisfy the specified color detection formula, the pixel is considered as black pixel; hence, a binary image of the ROI is produced. After completing the real-time processing on one frame, the image processing unit provides two types of data for two different outputs. Firstly, the R, G, and B components of the binary images that are controlled by the VGA controller are displayed on the VGA monitor. Secondly, the total number of pixels counted from an image frame that satisfies the specific color detection formula are determined.

A real-time data transfer unit was developed to transfer the total number of detected pixels to an external processor to record the percentage of an area that is detected as R, G, or B. Here, the universal asynchronous receiver and transmitter (UART) communication protocol, along with the

RS232 standard for serial communication, was used. The Cyclone IV FPGA family was provided with the ZT3232 transceiver chip, which was used for the real-time RS232 serial data transfer. Therefore, the number of pixels detected inside the ROI for one frame are transmitted via the RS232 port of the DE2-115 FPGA board. A field laptop with an Intel® Core™ i7 CPU @2.70 GHz processor, 4.00 GB RAM, and 64-bit Windows operating system (OS) was used to receive the serial pixel data and save the pixel area detected for further analyses. The functional block diagram for the real-time transfer unit is explained in Fig. 4.9.

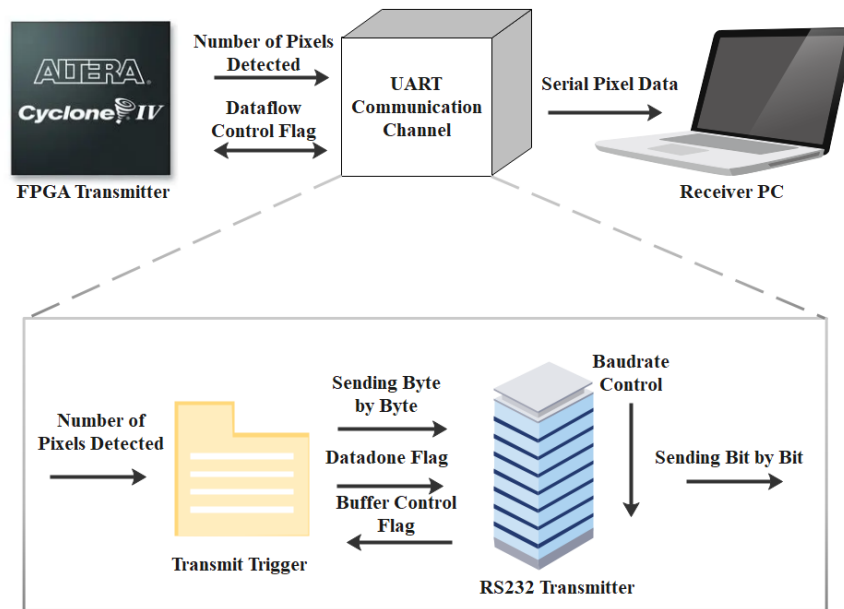


Fig. 4.9: The UART communication channel for real-time data transfer.

The transmitter software was designed using the Quartus Prime Lite 18.0 programming tool in a PC with Intel® Core™ i7-3770 CPU @3.40GHz processor, 16.00 GB RAM, and 64-bit Windows 10 OS. For this communication channel, two different modules, Transmit Trigger and RS232 Transmitter, were created in the same project directory as the image acquisition and image processing units. The detected pixel area from the image processing unit is a six digits number. The Transmit Trigger module inputs these six digits as six bytes and sends it to the RS232 Transmitter module, one by one, and maintaining a one-byte time interval. As the FPGA baud rate was selected

as 115,200 for this study, and the UART module was running with a 50MHz clock, one bit required $(50 \times 10^6) / 115200 = 434$ clock pulses. As a result, each byte (8-bits) from the six-digit pixel data, along with a start and stop bit, was sent at $(8 + 1 + 1) \times 434 = 4340$ clock pulses apart. Transferring the parallel bytes as a stream of serial data was controlled using two flag control registers (e.g., buffer control flag and data done flag) to avoid a data overflow error. Consequently, the RS232 transmitter module sends the received byte to the receiver PC on a bit-by-bit basis by following an interval of 434 clock pulses. The receiver software was designed using the Python programming language that was installed on the receiver PC by using the Anaconda navigator. The same Python programming interface was used to launch several Conda packages, such as *Spyder* and *PySerial*.

4.2.2. RTK-GPS System

The geolocation information (i.e., latitude and longitude) are an important factor of the decision support system that helps end-users to apply site-specific farm management solutions in the practical field. From the literature review of current PA solutions, it has been found that the accuracy of GPS is within a few meters, which is sometimes inefficient for weed patch identification and mapping on a field scale (Lamb & Brown, 2001). Hence, another component of this study was to focus on improving the real-time GPS, so the accuracy is within a few centimeters. For this purpose, two identical RTK boards from u-blox's M8 high precision positioning module were configured to serve as the RTK rover, and the RTK base station. Each board required the following three connections (Fig. 4.10): the GNSS patch antenna that responds to the radio signals from GNSS satellites to compute the position; the UHF whip antenna that provides maximum flexibility to assess GPS signals in the high-frequency range; and the micro-USB to provide both the 5-volt supply power and the configuration setup.

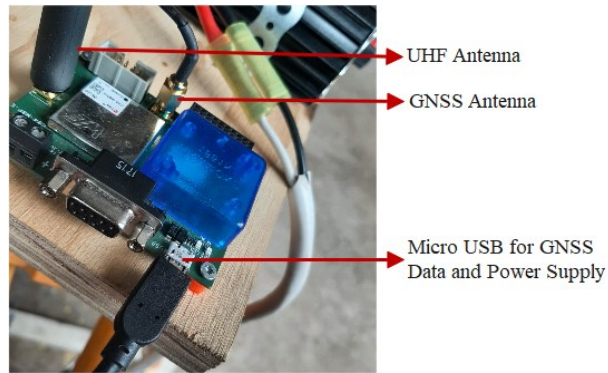


Fig. 4.10: The C94-M8P application board with necessary connections.

At first, the RTK base station was configured in the TIME mode by using the self-survey in facility of u-center 21.05 (u-blox Inc.; Thalwil, Switzerland) software with the minimum observation time of 86,400 sec (1 day) and required position accuracy 0.08 m (8 cm). However, the true observation time used to achieve 8cm accuracy was 178,964 sec (2 d, 1 hr, 42 min, 44 sec). Then, the RTK base station's radio link port was configured with a baud rate of 19,200. This radio link provided radio technical commission for maritime services (RTCM) correction messages to the RTK rover for GPS + globalnaya navigazionnaya sputnikovaya sistema (GLONASS) GNSS configuration. Once the base station was configured, one of the two identical RTK boards were covered inside a waterproof box, which included the waterproof antenna connection for both the GNSS and UHF. The waterproof box was installed on the wooden roof of the balcony of the treehouse building (45.374856152374974, -63.26396593073179) inside the campus area, which was situated at a distance less than 100 m from the selected test field. Finally, the RTK rover radio link port configuration with baud rate 19,200 was used to receive the RTCM correction messages from the RTK base station.

During field data collection with the RTK base station running on TIME mode, the RTK rover required several minutes to go into primarily RTK FLOAT mode, and finally RTK FIXED mode after receiving RTCM corrections and resolving carrier ambiguities. During the data

collection time, it was important for the RTK rover to be in the FIXED mode to provide accurate latitude and longitude. The functionality of the RTK-GPS is shown in Fig. 4.11.



Fig. 4.11: The communication among RTK base station, RTK rover, and the satellites.

4.3 Data Storing Unit

Among the necessary components of this real-time crop monitoring system, the DSU plays a significant role in establishing the software communication between the different hardware units using the physical ports from the PC (Fig. 4.12). The DSU is a laptop with an Intel® Core™ i5-8250U CPU @ 1.60 GHz-1.80 GHz x64-based processor running on the Windows 10 64-bit operation system. Python is the core programming language used to design and run the DSU to accumulate real-time data from the serial output of RFIP hardware, and RTK rover, and then geotags them with corresponding reference images of resolution 1920×1080 pixels using the USB connection with the web camera. The *piexif*, *PIL*, *cv2*, *pynmea2*, *serial*, and *fractions* Python packages were used. A free integrated development environment, Spyder from the Anaconda navigator desktop GUI, was used to write and run the Python scripts for data accumulation and storage.

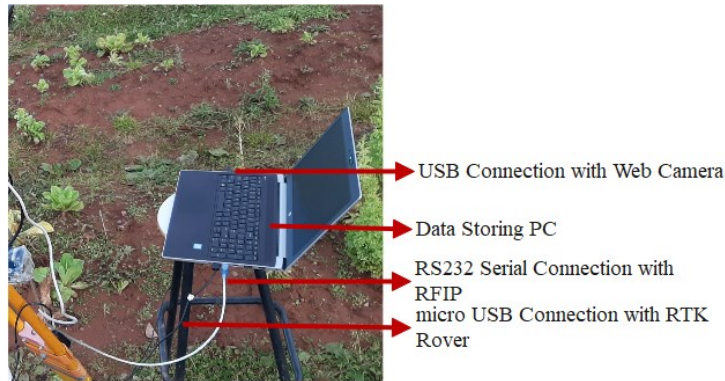


Fig. 4.12: Data storing PC with necessary connections.

The functional design of the DSU software included two different sub-functions, along with the main function. One of the subfunctions was designed to parse the GPS data and organize it in the specified format for geotagging with latitude and longitude metadata; whereby another was designed to maintain the 1920×1080 pixels web camera image resolution while saving the georeferenced field images. The main function was designed to read two serial ports (RFIP hardware unit and RTK rover) at different baud rates (115,200 and 19,200), which corresponded to the specified hardware units; and to run the web camera image stream simultaneously. Finally, the detected plant leaf area inside the $30 \text{ cm} \times 22.5 \text{ cm}$ wooden frame along with the latitude and longitude of that specific plant was geotagged as metadata during the field imagery. The georeferenced images of the selected spots were stored in a specified folder on the PC.

4.4 Post-Processing Unit

The PPU is needed to provide the farm management decision support results to the farmers. In most of the current, real-time, crop monitoring services, this step is time-consuming when analyzing field data. However, in this research, the RFIP prototype was developed to not only acquire the field images, but also process to the images and deliver the processed result in real-time. Therefore, the PPU only extracts the image metadata from the georeferenced field images

and stores the detected area with the corresponding GPS location in a specified format to be utilized by the WVL.

The PPU consists of the same PC and programming language as the DSU but uses different Python packages. The software component of the PPU is simpler than the DSU and was designed using only two Python packages: *piexif* and *PIL*. Furthermore, the script did not have multiple functions or layers. The saved image's Exif metadata was read and saved as a comma-separated value (CSV) file.

4.5 Performance Analysis and Visualization

The last section of the design was to analyze the performance of the RFIP system and visualize the geographic latitude and longitude collected using the RTK-GPS. For this purpose, the georeferenced data from the field monitoring were extracted in a specified format through the PPU. The detected pixel areas were compared with the reference data for performance analysis and the Google Earth Pro software was used to visualize the geolocations.

4.6 Testing of the System

4.6.1. Testing of the RFIP System – Lab Environment

The experimental setup for the lab evaluation of the RFIP system comprised of the DE2-115 FPGA development board, D8M camera board, the receiver PC, a VGA display monitor, a custom-built wooden frame, one additional DC light source with SMD2835 light-emitting diode (Vision Global Media Group Inc.; Waterloo, ON, Canada), and a digital lux meter from Aoputriver® (Fig. 4.14). The wooden frame consisted of a 122 cm × 61 cm base to place the test

object on, and a 152.4 cm × 5 cm vertical board to embed the DE2-115 FPGA board along with the D8M camera board.

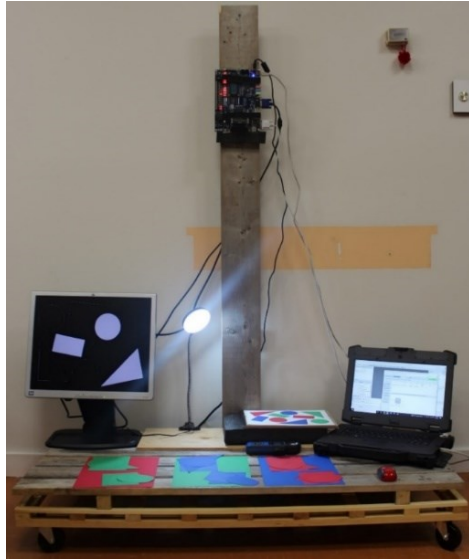


Fig. 4.14: Experimental setup of the RFIP system for lab evaluation.

To ensure a consistent lighting condition, the DC light and the AC light, installed in the lab ceiling, were used. Before testing the system, the same light intensity for each object was ensured, which was 600-601 Lux with a room temperature of 21-22°C. For evaluation purposes, several objects with different structures were formed using 28 cm × 22 cm color sheets. Here, the colors included re-entry red, gamma green, and blast-off blue (Astrobrights Inc.; Alpharetta, Georgia, USA; Fig. 4.15).

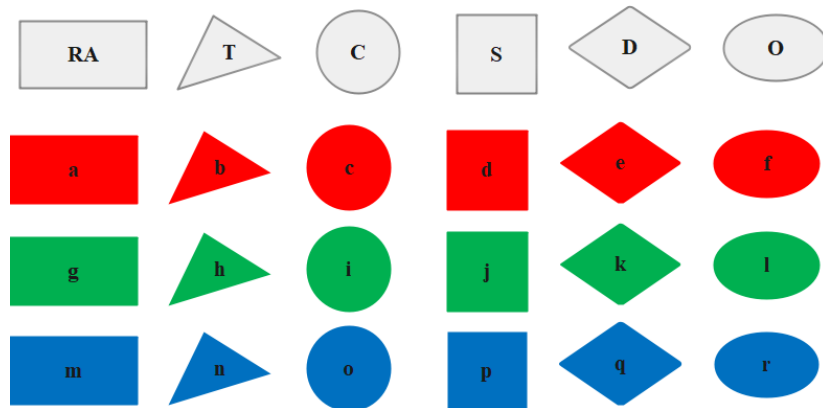


Fig. 4.15: Different shapes considered for objects to be detected.

To test the image processing unit, 16 objects with different shapes were made by resizing the three-color sheets (Table 4.2). In this experiment, rectangle (RA), triangle (T), circle (C), square (S), diamond (D), and oval (O) shaped objects were used with three different colors (R, G, and B) for all (Abbadi & Saad, 2013).

Table 4.2: Objects formation with shapes and colors for the performance evaluation of R-ratio, G-ratio, and B-ratio filter.

Objects	Shapes
1	a
2	b
3	c
4	a, b, c
5	d
6	e
7	f
8	d, e, f
9	a, g, m
10	b, h, n
11	c, i, o
12	a, g, m, b, h, n, c, i, o
13	d, j, p
14	e, k, q
15	f, l, r
16	e, j, r

4.6.1.1. Data Collection using the RFIP System

The RFIP system was mounted at 99 cm above the flat surface of the custom-built wooden frame for the data collection, where the different objects were placed for imaging. The D8M camera had an 800×600 pixels resolution, while the area covered on the ground was $27.5 \text{ cm} \times 21.5 \text{ cm}$. During the data collection period, 10 sets of pixel data were recorded for each 16 objects that resulted in 160 values for each color detection algorithm.

The data acquisition software was designed using Python programming language. Python script was written using a conditional while loop and a specific color detection formula to record 10 data samples from one object. The real-time processed data were saved in a text file.

4.6.1.2. Acquisition of Reference Data

To compare the performance of the developed RFIP system, a Canon EOS Rebel T3i EOS 600D DSLR camera with a Canon EFS Lens EF-S55-250 mm f/4-5.6 IS II was used (Canon Inc.; Ota City, Tokyo, Japan). During the acquisition of the reference images, the same experimental setup as the RFIP data collection was maintained. Here, the F-stop, exposure time, and ISO speed of the camera were maintained at f/5.6, 1/30 sec, and ISO-200, respectively.

After collecting all the reference images, they were cropped and resized to match the ROI area and resolution of the RFIP imaging system. Here, the Adobe Photoshop CC 2019 software (Adobe Inc.; San Jose, California, USA) was used to make the modifications so they matched the 27.5 cm × 21.5 cm ground area and the 800 × 600 pixels image resolution. Finally, all the reference images were saved in a file directory for data analyses. Lastly, the Python programming language was used to apply the corresponding color detection formulas on the 160 reference images to determine the reference pixel areas and save in a text file.

4.6.2. Testing of the RFIP System – Outdoor Environment

To evaluate the effectiveness of the RFIP system in the outdoor environment, the system was tested at the Agricultural Campus of Dalhousie University, Truro, Canada (45.374°N, 63.264°W). The data collection unit was placed as stationary unit, which included the following:

the RFIP system, installed on the custom-built T-shaped wooden frame and placed on top of a tripod; the battery and inverter to supply power; the PC to store collected data; the live streamer CAM 313 (PW313) 1080p web camera (AverMedia Inc.; New Taipei City, Taiwan) to collect the reference images; and other necessary cables (Fig. 4.16). The D8M camera was placed 29 cm down from the tripod top, and 121 cm above the object, and the web camera was placed 82 cm down from the tripod top and 68 cm above the object. Two legs of the tripod were 152.4 cm, and one was 139.70 cm in length. The size of the container that carried the objects was 34.29 cm × 29.21 cm, and the wooden frame used to maintain 800 × 600 pixels image resolution of the RFIP system from 121 cm was 30 cm × 22.5 cm, in size.

The date by which the system was tested was selected based on the weather conditions. The test occurred on a day with a clear, and bright day with a temperature of 15°C, a wind speed of 17 km/h, a humidity of 72%, and an atmospheric pressure of 100.6 kPa. A location was selected where there was consistent shade and lighting intensity of 3900-4000 Lux.



Fig. 4.16: Field data collection setup to validate RFIP system in the outdoor environment.

For data collection purposes, 22 Romaine lettuce live plants were collected from the field and placed inside the container having soil on the same data collection date to create a field prototype and avoid system movements in the primary validation stage. From each plant using the python programming tool, a total of 10 data samples were collected as the RFIP detected pixel area using the G-ratio detection formula, and 10 reference images using the web camera. Finally, 220 processed data from the RFIP system were saved in a text file. Next, the 220 reference images were cropped by using the custom-built blue frame to match with the same ground resolution as the RFIP system and processed using the same formula as used by the RFIP system to detect plant leaf area, to generate the same set of 220 reference data for performance evaluation. A sample of object detection procedure is pictorially depicted in Fig. 4.17.

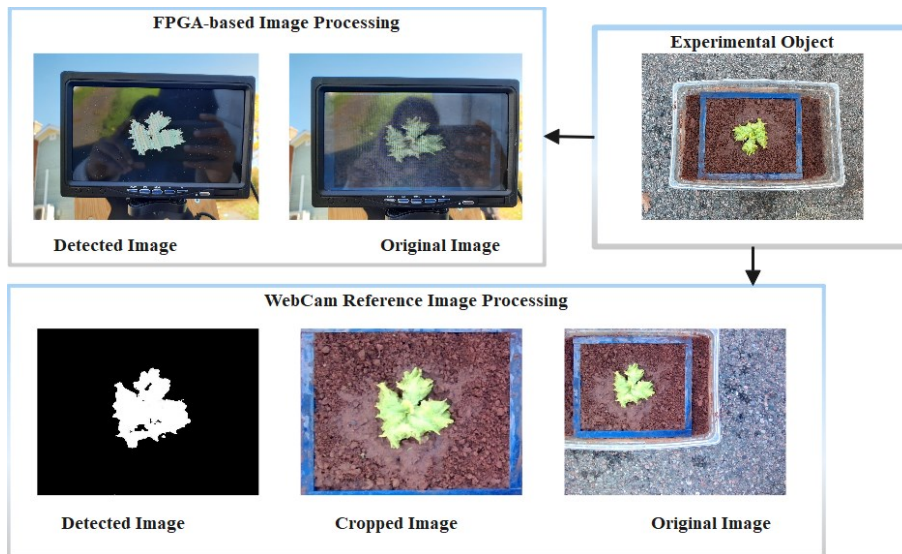


Fig. 4.17: Sample of object selection and detection technique.

4.6.3. RTK-GPS Accuracy

The experiment performed in this case was to check the accuracy of the RTK-GPS system in the 8 cm scale by collecting the real-time geographic locations from the selected spots. Though

the total system needed to be carried and placed on the selected field points, the data were recorded in the stationary mode to avoid human errors.

To see the positioning accuracy of the RTK rover at 50 cm, 30 cm, 25 cm, and 20 cm after responding to the correction messages from the RTK base, four spots were selected (Fig. 4.18) within 50 m distance from the RTK base station. The GPS data of RTK rover were recorded using u-center 21.05 GNSS evaluation software, ensuring the FIXED status on the rover. Later, Google kml files were generated from the four recorded data files using the u-center software to visualize the recorded GPS data on a real-time Google map through Google Earth Pro software.

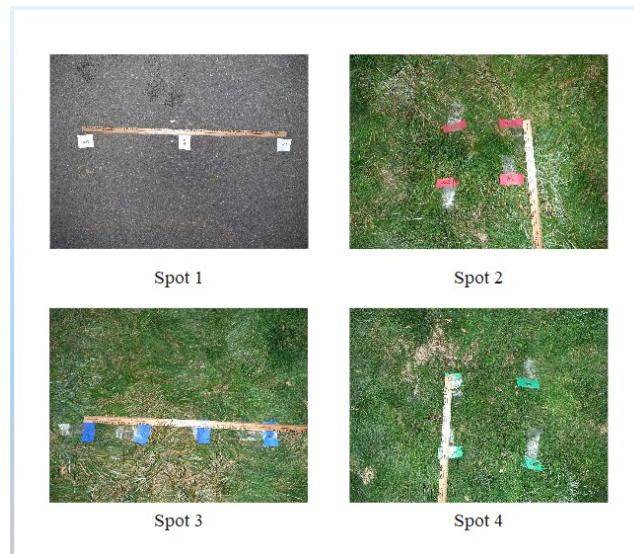


Fig. 4.18: The test spots (with scale to assist measurements) for RTK rover's 8 cm accuracy evaluation.

4.6.4. Testing of the Real-time Crop Monitoring System

To test the real-time crop monitoring system, Dalhousie University's Demonstration Garden (45.3755°N, 63.2631°W) was used as a testing site, which was located within the 100 m range of the RTK base station. For the field experiment, 21 Romaine lettuce plants were selected from three crop rows (7 plants in each row; Fig. 4.19). Due to the automatic exposure control

limitation of the RFIP system, field data was acquired when the weather status showed conditions that were clear, mainly sunny, or with few clouds. To avoid the effects of cloud on the plants and maintain a consistent brightness during the data collection period, an umbrella was used to provide shade for all the sample points. Accordingly, the analog gain, digital gain, and exposure gain parameters were chosen to deliver the best detection results under the sun with shading provided by the umbrella.

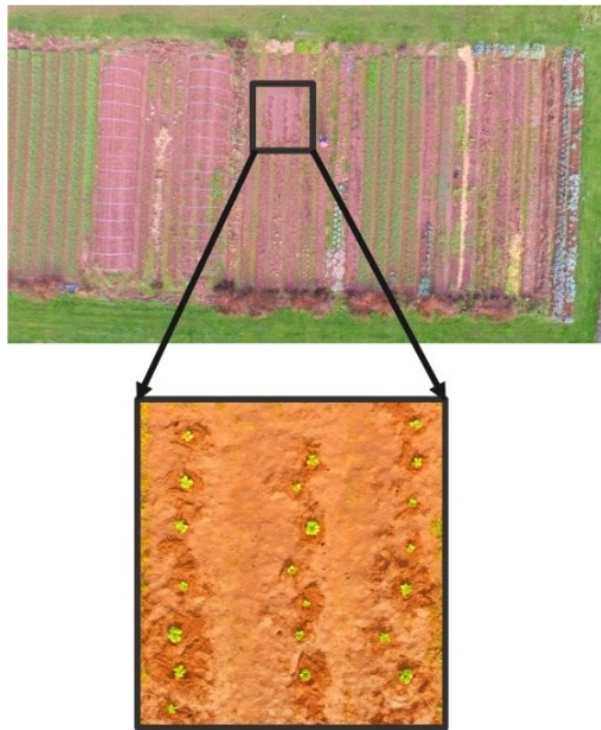


Fig. 4.19: Selected site for field data collection inside the Dal-AC. demonstration garden.

According to the primary outdoor data collection prerequisites from the RFIP system's evaluation in the outdoor environment, several important factors were considered during field data collection. Firstly, by keeping track of the weather status, a mainly sunny day was chosen (temperature: 4°C; wind: 14 km/h NW; wind gust: 30 km/h). Secondly, a large outdoor umbrella (7.5 ft), and a small rain umbrella were chosen to create a consistent shade and mitigate the cloud effects over the plant areas. For the field evaluation, the RTK-GPS was added with the RFIP

system. The complete system (Fig. 4.20) was moved and adjusted by changing the lengths and angles of the tripod's three legs to maintain the same ground resolution of $30 \text{ cm} \times 22.5 \text{ cm}$ with 800×600 pixels image resolution for each of 21 data points. From each data point, a total of 7 samples were collected which resulted in a total data set of 147 samples.



Fig. 4.20: Field data collection setup for the validation of real-time crop monitoring system.

The field data were collected from two serial outputs: the latitude and longitude with the RTK rover in FIXED mode; and the pixel area detected as a plant. These data were geotagged as image metadata with the web camera reference image of corresponding data points by maintaining 1920×1080 pixels resolution to facilitate the cropping and resizing of the reference images to match with the RFIP imagery. The cropped and resized reference images were processed to find 147 reference pixel areas using the *NumPy* and *cv2* packages in Python. The Python script was written to perform mathematical operation on the reference images, pixel by pixel by following the G-ratio formula.

After the field monitoring, the RFIP data and the RTK-GPS data were extracted from the geotagged reference images and saved as a CSV file. The RFIP data from the CSV file were compared with reference data collected using the web camera for the performance evaluation. On the other hand, the latitude and longitude values from the CSV file were used by the Google Earth Pro software to visualize the selected data points for field evaluation on the Google map.

4.7 Performance Evaluation of the System

4.7.1. Performance Evaluation of the RFIP System in the Lab and the Outdoor Environment

The DSLR and Web Camera imagery were used to compare and evaluate the performance of RFIP system, as these two image acquisition sources have been widely used in real-time image processing systems over the past few years (Das, 2020; Rehman, et al., 2018; Shin, et al., 2020). Since this research focused on providing cheaper, faster, and reliable real-time image processing system alternative, the performance of the developed system was compared with high end image acquisition systems. Statistical analysis related to the acquired data were carried out in Minitab 19 (Minitab Inc., State College, Pennsylvania, USA), Excel (Microsoft Inc.; Redmond, Washington, USA) and Python. Basic statistical analysis was performed to evaluate the developed system, whereby the mean, standard deviation (SD), and the percentage root mean square error (RMSE) of the detected pixel area (Eq. 4) were the main metrics for comparison.

$$(\%RMSE = \frac{RMSE \text{ in Pixel}}{Total \text{ Pixel Area Considered}} \times 100\%) \quad (\text{Eq. 4})$$

For the lab evaluation of the RFIP system, there were 10 samples per 16 objects, resulting in a total of 160 samples from the RFIP system and 160 samples from the DSLR reference system for each of the three corresponding ratio algorithms. The RFIP data and DSLR data were averaged using 10 samples for each object in a total of 48 combinations were computed for the RFIP data and DSLR data respectively including three color ratio algorithms ($16 \times 3 = 48$). For the outdoor evaluation of the RFIP system, there were 10 samples per 22 plants, resulting in a total of 220 samples from the RFIP system and 220 samples from the web camera reference system. The RFIP data and web camera data were averaged using 10 samples for each plant to get 22 samples for each system. These data were analyzed and compared using the G-ratio algorithm for the real-time detection in the outdoor environment.

The detected areas determined from the RFIP system were correlated with the areas detected using the DSLR and the web camera via regression analysis. Lin's concordance correlation coefficient (CCC) from the lab and outdoor test results were calculated and used to measure the accuracy between the RFIP data and the reference data (Lin, 1992). For hypothesis testing, Lin (1992) indicates that rather just testing whether CCC is zero, it is more logical to test whether CCC is greater than a threshold value, CCC0. The threshold was calculated using the following equation (Eq. 5), where X_a is the measure of precision (calculated using the formula mentioned in Eq. 6, where ν and ω were the functions of mean and standard deviation), ρ^2 represents the R-squared achieved when the RFIP data was regressed on the reference data, and d is the % loss in precision that can be tolerated (Lin, 1992).

$$CCC0 = X_a \sqrt{\rho^2 - d} \quad \text{Eq. 5}$$

$$X_a = \frac{2}{v^2 + \omega + \frac{1}{\omega}} \quad \text{Eq. 6}$$

This is analogous to a non-inferiority test of CCC. The null and alternative hypotheses are H0: CCC ≤ CCC0 (there is no significant concordance between the RFIP data and the reference data) and H1: CCC > CCC0 (there is a significant concordance between the RFIP data and the reference data). If CCC > CCC0, the null hypothesis is hence rejected, and the concordance of the new test procedure is established. Also, the RMSE was calculated and used to compare the performance of the RFIP system with the reference systems using same algorithms. As the RFIP system was a combination of image acquisition and image processing systems, the reference images acquired were processed pixel by pixel using Python by applying the same algorithms used in the RFIP system's image processing unit.

4.7.2. Performance Evaluation of the RFIP System in the Field Environment

To evaluate the RFIP system during the field trial, the same analytical tools and metrics were used. Before the performance comparison of the RFIP system with the web camera reference system from the field experiment, an empirical correction factor was used on the RFIP detected areas, to compensate for the effects of illumination conditions, observation geometry, and atmospheric phenomena on the spectral signatures of objects (Teillet, 2007). An empirical correction factor can be applied on a data set to provide the best estimate of the acquired data with a minimized error (Davies, 2001). Here, an empirical correction factor of 0.6 was used to find the corrected RFIP area from the detected RFIP area during field trial (Ogier et al., 2007).

For the field evaluation of the RFIP system, there were 7 samples per 21 plants, resulting in a total of 147 samples from the RFIP system and 147 samples from the web camera reference system. The RFIP data and web camera data were averaged using 7 samples for each plant to get 21 samples for each system. The data were analyzed and compared using the G-ratio algorithm for real-time detection in the field environment. The detected areas in pixels collected using the RFIP system were corrected using the selected empirical correction factor and the corrected RFIP areas were correlated with the areas detected by web camera using regression analysis. Lin's CCC was calculated to measure the accuracy between the corrected RFIP data and the reference data in the field environment. For the hypothesis testing, the CCC was compared with the CCC0 as stated in section 4.7.1 from the field test results to find the significant concordance between the corrected RFIP data and the reference data in the field environment (Lin, 1992). To compare the field performance of the RFIP system, RMSE was also calculated and used. The reference images acquired from field monitoring were processed pixel by pixel using Python by applying the same algorithm used in the RFIP system's image processing unit.

CHAPTER 5. RESULTS AND DISCUSSION

5.1 Results

The results of the prototype were the plant leaf areas detected from the ROIs and the corresponding geolocations of the selected spots from field monitoring. The geographic locations of all selected points along with the detected pixel areas on those locations were geotagged during field monitoring by using the real-time crop monitoring system. The geolocations were acquired using the RTK-GPS with 8 cm positional accuracy and the detected pixel areas were acquired using the serial data transfer module of the RFIP system. The geotagged data were extracted from the field images during post-processing for the performance evaluation and visualization. The 16 color objects were selected for lab experiment, 22 Romaine lettuce plants were selected for outdoor experiment, and 21 Romaine lettuce plants were selected for field experiment.

5.1.1. Experimental Results of Lab Evaluation

The outputs of the RFIP system from the lab experiment consisted of the number of pixels detected as R, G, or B by applying color detection algorithms. The detected pixel areas were compared with the pixel areas detected from the reference images captured by the DSLR camera maintaining the same experimental setup as the RFIP system. The numerical representation of the complete data with all the resulting numbers is shown in Table 5.1 for the three ratio filters.

Table 5.1: Number of pixels detected from the ROI area along with the SD for 16 objects using three-color ratio filters.

Object/ Algorithm	Red Ratio		Green Ratio		Blue Ratio	
	RFIP Data	DSLR Data	RFIP Data	DSLR Data	RFIP Data	DSLR Data
1	134151.80±	130136.40±	129375.30±	128983.70±	125053.40±	128860.60±
	834.41	585.13	117.15	416.84	224.35	522.42
2	95945.29±	90020.60±	91250.84±	89730.70±	87393.63±	89642.60±
	559.21	433.29	180.95	430.43	210.37	243.12
3	83379.30±	76736.70±	78565.35±	76243.10±	73506.82±	76120.40±
	724.86	239.39	58.75	185.45	4204.90	226.45
4	85048.98±	77680.10±	80049.29±	77401.80±	75687.72±	77395.10±
	150.66	242.57	112.62	491.16	123.49	346.25
5	88135.14±	80491.30±	83603.98±	80598.40±	79938.65±	81393.40±
	544.02	316.36	257.07	213.01	408.07	466.21
6	58291.06±	49540.60±	54033.82±	50168.00±	48966.72±	49049.80±
	846.56	403.84	74.60	137.73	85.94	141.46
7	52463.82±	43343.50±	47350.33±	43074.30±	43262.76±	42958.90±
	936.82	314.96	49.76	197.56	82.77	143.41
8	177685.10±	173227.40±	174745.90±	173506.00±	169075.20±	173244.60±
	456.34	594.43	640.63	705.79	1092.86	703.39
9	33582.16±	23505.40±	28999.28±	23541.60±	24382.31±	23467.50±
	664.40	153.50	206.07	112.58	182.88	131.55
10	42318.15±	29399.40±	35727.60±	29252.10±	30478.85±	29380.90±
	1218.94	285.42	69.68	104.37	296.90	193.23
11	36895.99±	24987.20±	30869.18±	24572.70±	25698.35±	24722.00±
	1985.01	642.13	342.36	120.14	321.88	92.57
12	87487.72±	77107.80±	81759.20±	76909.40±	76172.50±	77492.80±
	1109.38	471.15	940.22	356.59	311.27	352.62
13	90208.14±	80244.90±	84924.05±	80535.10±	79265.16±	81525.50±
	521.19	337.83	518.82	343.73	1394.427	522.96
14	60431.49±	49255.30±	54687.74±	49952.10±	48963.39±	48928.50±
	750.09	187.37	278.97	287.92	1543.55	198.09
15	53714.00±	43303.30±	48004.31±	43184.10±	43602.31±	43300.30±
	271.81	246.39	397.67	143.53	993.33	224.30
16	60697.53±	49413.80±	84488.80±	80210.20±	44202.75±	43158.60±
	74.67	241.26	844.14	343.71	248.94	164.38

From the statistical analysis, the variability in SD of the 16 objects from RFIP system was found to be considerably low ($0.074\% < SD < 5.72\%$), which implied the consistent behavior of the imagery system. Thus, during the lab trials using the controlled luminance conditions (600-601 Lux) with a constant height from the objects, the RFIP system performed well in terms of plain color object detection (See Table 5.2 for the representation of the variation of SD using three different color ratio filters).

Table 5.2: Percentage of deviation for three-color ratio filters.

Ratio Filter	SD (% w.r.t the total ROI)	
	Minimum	Maximum
Red	0.123	5.38
Green	0.074	1.15
Blue	0.163	5.72

The results from lab evaluation are shown as bar charts in Figs. 5.1, 5.2, and 5.3. The bar charts of three different color ratio filters explain the consistent performance of the RFIP system's image sensor compared to the DSLR reference system for R, G, and B color objects detection from a defined ROI with minimal noise.

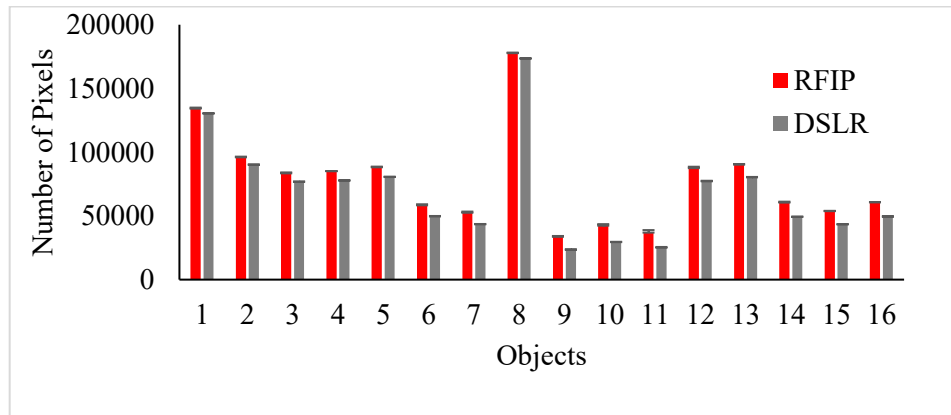


Fig. 5.1: Comparison between pixels detected as red using the RFIP system and the DSLR reference imaging system.

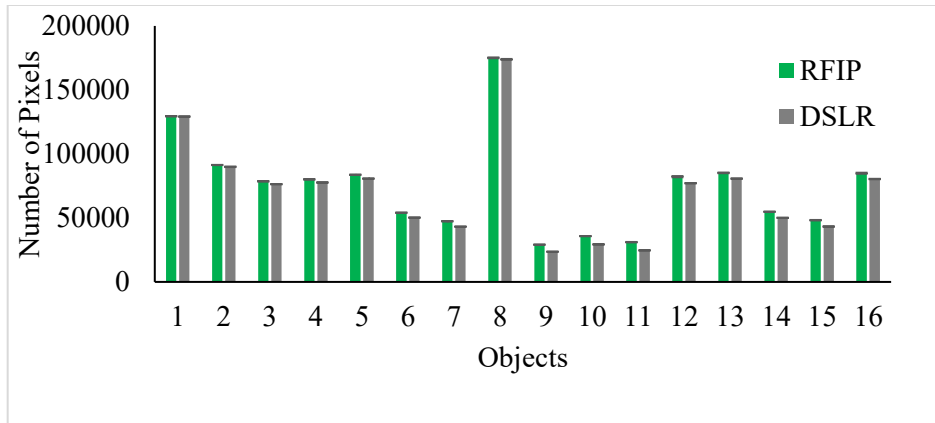


Fig. 5.2: Comparison between pixels detected as green using the RFIP system and the DSLR reference imaging system.

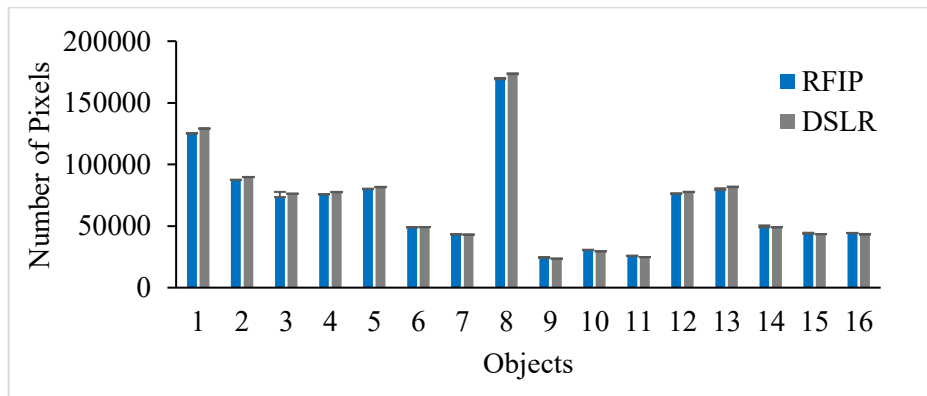


Fig. 5.3: Comparison between pixels detected as blue using the RFIP system and the DSLR reference imaging system.

The performance of the RFIP system was compared with the DSLR based system for R-ratio, G-ratio, and B-ratio algorithms using regression analysis. The detected area using the RFIP system was found to have a strong correlation with the DSLR imagery-based system (RFIP=1.0327 DSLR; $R^2=0.9956$; RMSE=6019.9230 Pixels; $n=480$; $p\text{-value}<0.05$), which implies that the RFIP system could be used to explain 99.56% variability in the area detected using the DSLR (Fig. 5.4) with a substantial accuracy (CCC = 0.9873). Also, a 1:1 trend line was generated in Fig. 5.4 to visualize the performance of the RFIP system and compare it with the ideal system. It was shown that the RFIP system performed considerably well for color object detection from a selected ROI.

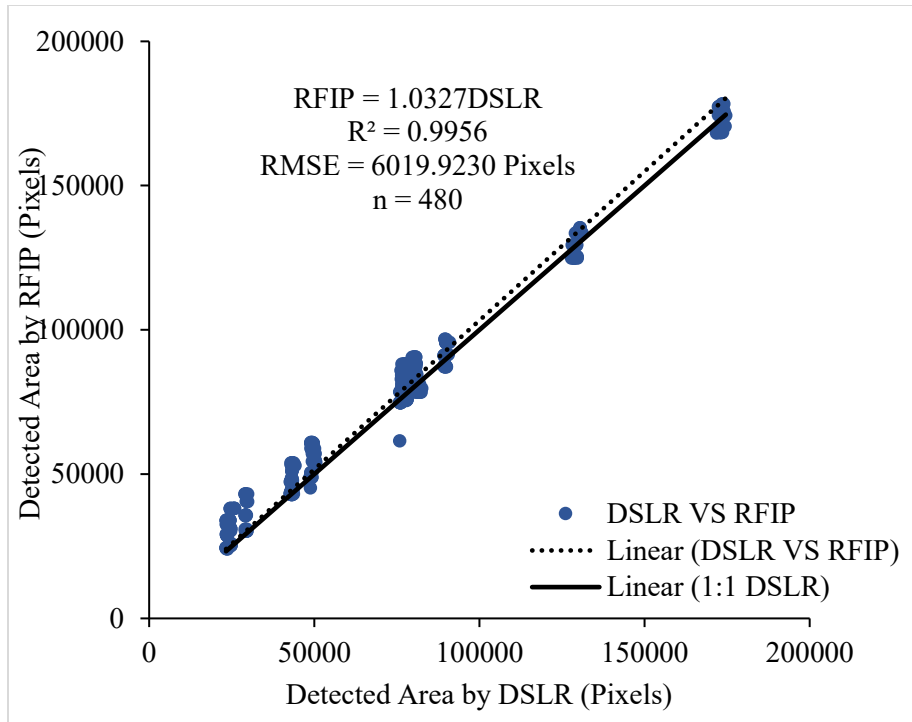


Fig. 5.4: Correlation between ground truth detected area using the DSLR and actual detected area using the RFIP system (RFIP=1.0327DSLRL; $R^2=0.9956$; RMSE=6019.923 Pixels; n=480; $P<0.05$).

The RMSE was used to measure the deviation between the observed area (i.e., pixel area detected using the web camera system) versus the predicted area (i.e., pixel area detected using RFIP system) using three color detection algorithms (i.e., R-ratio, G-ratio, and B-ratio). Here, the RMSE for detected pixel area was only 1.25% of the total pixel area considered, which also explains a better fit of the model. From the hypothesis testing using Eqs. 5 and 6, CCC0 is 0.9665 with a tolerable 5% loss of precision, whereas Lin's CCC = 0.9873 with the confidential interval 95% (0.9852; 0.9893). As the lower limit of CCC>CCC0, the test is statistically significant, and the null hypothesis is hence rejected. Therefore, the results from the lab trials depicts that the RFIP system can be used to predict the area detected using DSLR system.

5.1.2. Experimental Results of Outdoor Evaluation

The outputs of the RFIP system from the outdoor experiment consisted of the number of pixels detected as Romaine lettuce plant leaf area by applying the green color detection algorithm. The detected plant leaf areas were compared with the detected areas from the reference images captured by the web camera, which maintained the same experimental setup as the RFIP system (Table 5.3).

Table 5.3: Number of pixels detected using the RFIP system and the Web Camera imaging system from the ROI area along with the SD for 22 objects (Romaine lettuce plants).

Objects	Green Ratio	
	RFIP_Area	Web Camera_Area
1	49166.00±161.66	47486.00±444.48
2	77899.00±201.11	55160.10±157.08
3	56169.30±184.08	87778.30±806.07
4	59309.40±244.86	59048.50±253.32
5	103772.50±284.45	66557.00±130.09
6	62601.40±111.62	123096.60±560.73
7	55114.70±185.37	69735.30±252.44
8	111721.70±288.07	62462.10±136.29
9	54093.70±165.00	125856.40±418.17
10	109164.80±251.19	59904.00±192.54
11	75281.00±267.19	124714.70±523.44
12	54974.80±184.18	84839.10±359.07
13	73511.60±310.23	61213.60±285.60
14	52212.20±129.06	81856.70±304.31
15	51257.60±208.61	56741.80±240.93
16	75015.70±236.80	58214.80±255.57
17	75490.70±209.60	82448.20±368.71
18	78750.50±215.44	84037.70±464.33
19	73722.60±222.06	89323.70±358.14
20	91987.70±245.64	84770.30±259.95
21	51590.80±228.49	102659.20±257.67
22	49166.00±161.66	56940.80±189.22

From the statistical analysis, the variability in SD of the 22 objects (Romaine lettuce plants) from the RFIP system were found to be considerably low ($0.023\% < SD < 0.064\%$). The minor variability in the RFIP imagery system for the outdoor environment also implied the same consistent behavior as the lab environment. Thus, during the outdoor trials, the RFIP system performed well in terms of plant leaf area detection.

The results from outdoor evaluation are shown as bar chart in Fig. 5.5. The bar chart explains the consistent performance of the RFIP system's image sensor compared to the web camera reference system for plant leaf area detection from a defined ROI with minimal noise.

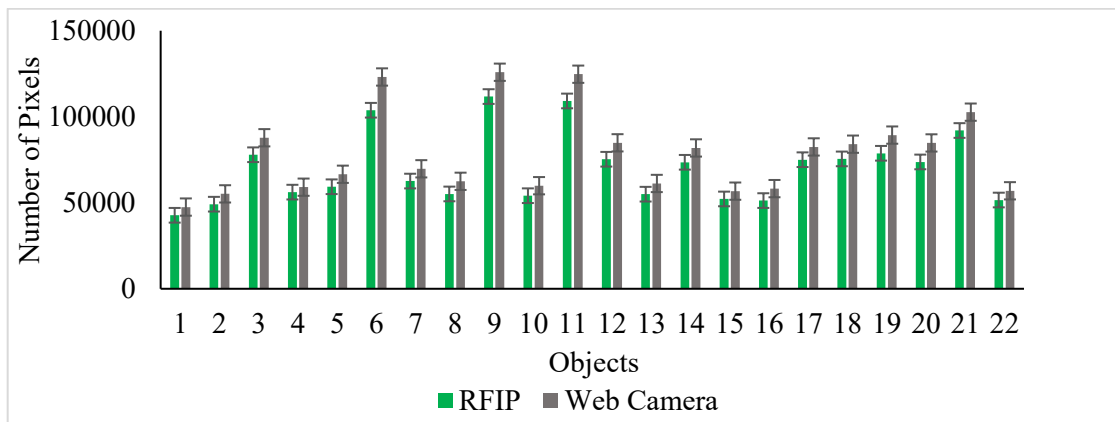


Fig. 5.5: Comparison between pixels detected as green (the plant leaf area) using the RFIP system and the Web Camera reference imaging system.

The performance of the RFIP system was compared with the web camera reference system for G-ratio algorithm (as the green plant leafage area detection is our concern) using regression analysis. The area detected by RFIP system had a strong correlation with the web camera system (RFIP=0.8868 Web Camera; $R^2=0.9994$; RMSE=9409.5910 Pixels; $n=220$; $p\text{-value}<0.05$) which showed that the RFIP system could explain 99.94% variability in area detected using the web camera (Fig. 5.6) with a moderate accuracy (CCC = 0.9101). Similar to the hypothesis testing for lab evaluation using Eqs. 5 and 6, CCC0 is 0.8894 with a tolerable 5% loss of precision for the outdoor evaluation, whereas Lin's CCC = 0.9101 with the confidential interval 95% (0.8945;

0.9257). As the lower limit of $CCC > CCC_0$, the test is statistically significant, and the null hypothesis is hence rejected. Therefore, the concordance of the new procedure is established.

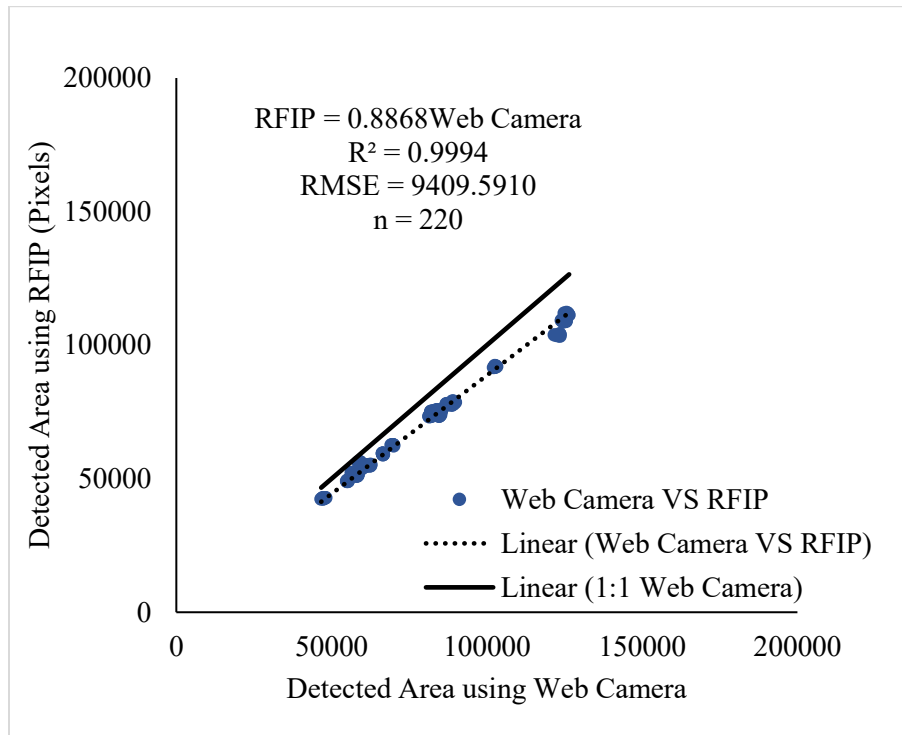


Fig. 5.6: Correlation between ground truth detected area using the Web Camera and actual detected area using the RFIP system (RFIP=0.8868 Web Camera; $R^2=0.9994$; RMSE=9409.591 Pixels; n=220; $P<0.05$).

A low RMSE, 1.96% of the total pixel area was observed for detected pixel area in the outdoor experiment. This was only 0.7% higher than the RMSE found in the lab experiment. This could have been caused by pixel noise in images captured by the RFIP's image sensor due to the exposure and brightness adjustments. The movement of leaves due to outdoor wind effect may be another reason for this. There may also have influences related to illumination conditions, observation geometry, atmospheric phenomena, and topographic variations on the spectral signatures of objects (Tillet, 2007).

5.1.3. Visualization of the Data Collected using RTK-GPS

The RTK-GPS data collected from the selected four spots during experiment were visualized using Google Earth Pro software to see the performance of the RTK-GPS in the 8 cm-scale. The spots were selected at the distances of 20 cm, 25 cm, 30 cm, and 50 cm. From the Google Earth Pro map visualization in Fig 5.7, the selected lines and squares from the experimental setup can be identified easily, which shows that the configured RTK-GPS showed a great performance to locate geographical places.

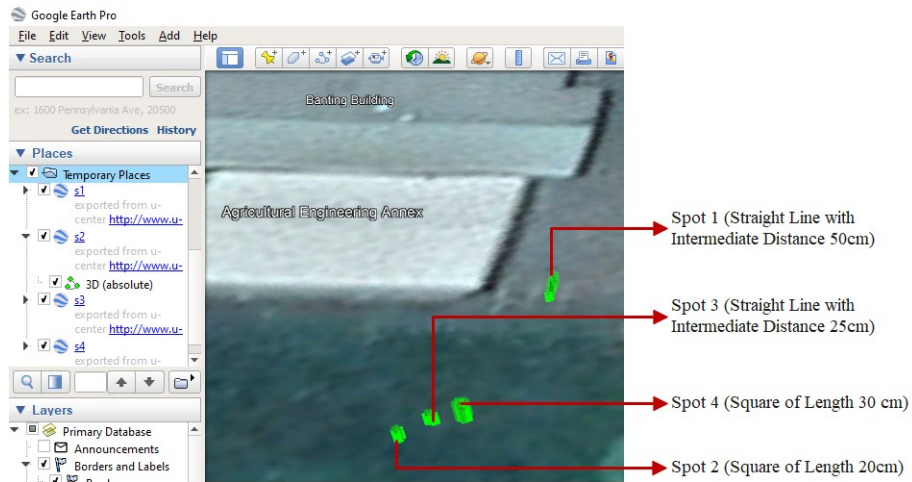


Fig. 5.7: The GPS data from four spots was recorded and utilized to visually represent the spots which are practically situated in the cm-scale.

5.1.4. Experimental Results of Field Evaluation

The outputs from the real-time crop monitoring system during field trial were the detected plant leaf areas using the RFIP system and the corresponding geolocations acquired by the RTK-GPS. The geolocations of 21 Romaine lettuce plants selected for field evaluation were visualized using Google Earth Pro software (Fig. 5.8) and the RFIP detected areas (i.e., after applying the empirical correction factor) were compared with the reference images captured by the web camera (Table 5.4).

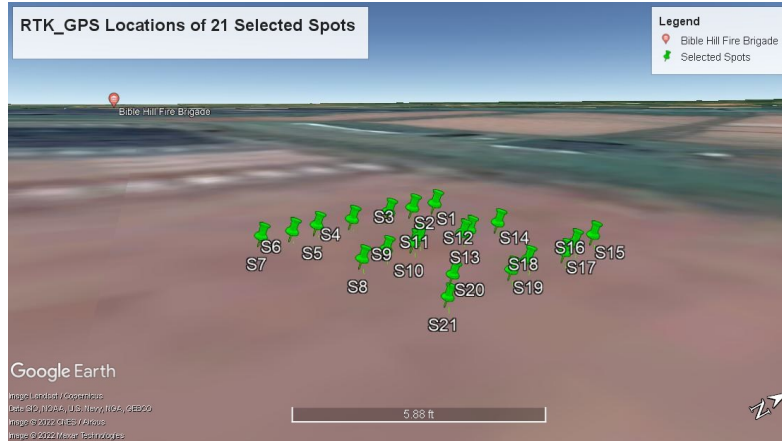


Fig. 5.8: The geolocations recorded using RTK-GPS with 8 cm accuracy.

From the statistical analysis, the variability in SD of the 21 objects (Romaine lettuce plants) from the RFIP system were found to be low ($0.16\% < SD < 9.13\%$). The minimal variability of the RFIP imagery system when tested in the field also implied the same consistent behavior as the outdoor test. Thus, during the field trials, the RFIP system performed well in terms of plant leaf area detection.

Table 5.4: Number of pixels detected from the ROI area along with the SD using G-ratio filter.

Objects	Green Ratio	
	RFIP Area_C [#]	Web Camera Area
1	99500.86±2975.46	112202.14±3355.28
2	133251.58±1853.85	150261.14±2090.49
3	149574.40±2806.92	168667.57±3165.22
4	87973.35±3253.62	99203.14±3668.95
5	187911.15±3949.76	211898.00±4453.95
6	149632.68±4542.97	168733.29±5122.88
7	90462.21±2361.17	102009.71±2662.57
8	131113.63±2294.10	147850.29±2586.95
9	97023.14±5792.45	109408.14±6531.86
10	84748.44±2119.82	95566.57±2390.41
11	116169.91±39988.54	130999.00±45093.08
12	195786.56±43865.01	220778.71±49464.38
13	97729.65±1204.94	110204.83±1358.75
14	155712.58±1865.83	175589.29±2104.00

15	118727.57±2032.01	133883.14±2291.39
16	99896.88±2989.09	112648.71±3370.65
17	103515.78±2545.09	116729.57±2869.97
18	103127.87±3014.13	116292.14±3398.89
19	132469.68±2011.39	149379.43±2268.15
20	101992.89±1573.79	115012.29±1774.68
21	167663.98±785.23	189066.29±885.47

#To compensate for the discrepancies during field experiment, RFIP Area_C data set was predicted from the RFIP Area data set, using an empirical correction factor (Ogier et al., 2007).

The results are shown as bar chart in Fig. 5.9. The bar chart also shows the consistent performance of the RFIP system's image sensor when compared to the web camera reference system for detecting plant leaf area in the field.

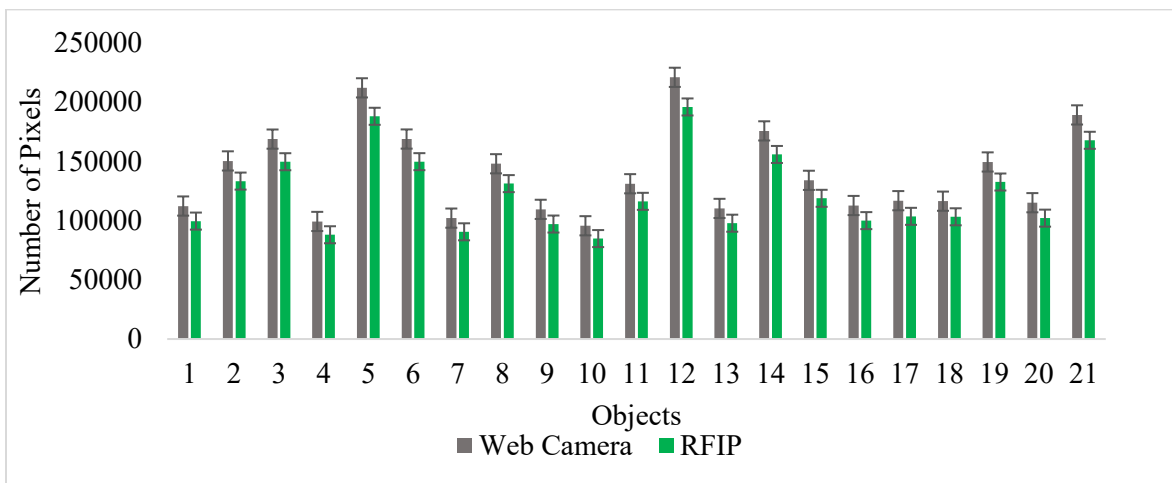


Fig. 5.9: Comparison between pixels detected as green (the plant leaf area) by the RFIP system and the Web Camera reference imaging system.

Similar to the outdoor evaluation, the area detected by the RFIP system (i.e., after applying the empirical correction factor) had a strong correlation with the web camera reference system (RFIP_C=0.9608 Web Camera; $R^2= 0.9566$; RMSE=30281.6600; n=147; p-value<0.05), which showed that the RFIP system could explain 95.66% variability in area detected using the web camera (Fig. 5.10) with a least moderate accuracy (CCC = 0.8236) during field monitoring. From

the hypothesis testing for field evaluation using Eqs. 5 and 6, CCC0 is 0.8521 with a tolerable 5% loss of precision, whereas Lin's CCC = 0.8236 with the confidential interval 95% (0.7876; 0.8595). As the upper limit of CCC > CCC0, it rejects the null hypothesis and established the concordance of the new procedure.

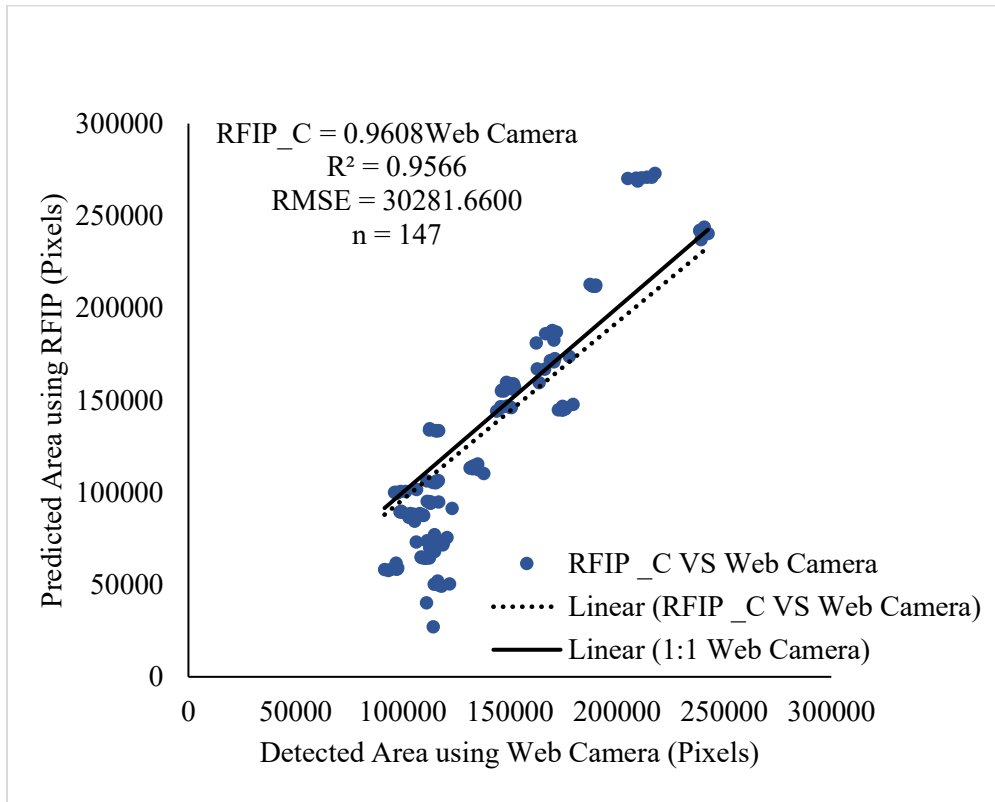


Fig. 5.10: Correlation between ground truth detected area using the Web Camera and predicted detected area using the RFIP system (RFIP_C=0.9608 Web Camera; R²=0.9566; RMSE=30281.66 Pixels; n=147; P<0.05).

From the field trial, an RMSE of 6.31% was measured for detected plant leaf area using the empirical correction factor, whereas 13.34% was measured without correction. Hence, a reduction of 7.03% in the RMSE was achieved by applying the empirical factor to the detected RFIP area during field trial.

5.2 Discussion

The RFIP system was able to acquire imagery at a higher resolution (800×600 pixels) during the lab, outdoor, and field trials than previous literature (Bannister et al., 2005; Cointault et al., 2012; Price et al., 2006; Ramirez-Cortes et al., 2013; Zhai et al., 2011). Furthermore, the integration of image acquisition and processing on a lightweight FPGA platform for PA crop monitoring purposes was effective in meeting current needs of local processing for real-time farm management decision support systems (Saddik et al., 2021). The RFIP demonstrated its effectiveness by providing 98.73% accuracy during the lab test, 91.01% accuracy during the outdoor test, and 82.36% accuracy during the field test, which were nearly closed to the detection rate achieved by Zhai et al. (2011) for another field of study related to license plate detection.

Evaluation Methods	SD (%)		RMSE (%)	CCC (%)
	Min	Max		
Lab	0.07	5.72	1.25	98.73
Outdoor	0.02	0.06	1.96	91.01
Field	0.16	9.13	6.31	82.36

Table 5.5: Summary of performance analysis.

By looking at the summary of performance analysis (Fig. 5.11), the RFIP system performed better in the outdoor experiment than the real crop field experiment. The reasons could be related to the effects of wind and the shadow over the ground ROI. Also, a greater number of replications for each object (10 samples per object for outdoor evaluation and 7 samples per object for field evaluation) may have had an influence on the analysis.

The RTK-GPS accuracy was precise enough to locate the field data points on the real-time Google map. However, from the scatter plots shown in the results section, there was a slight under-

or-overestimation for the object area detection during the experimental trials. The potential reasons could be the manually adjusted exposure and brightness of the image sensor; the value chosen for the threshold filter; and the luminance effects on the ROI. A slight under-or-overestimation is a common discrepancy in remote sensing technology (Silván-Cárdenas & Wang, 2008; Sayer et al., 2020), which did not have a major impact in this specific research.

Since the prototype was tested in the selected crop field to detect plant leaf areas, a single plant was chosen inside the defined ROI avoiding any weeds and unwanted empty areas. However, there were still unavoidable situations, which may have influenced data collection during the experimental phase. For example, the motion effect of the researcher on the experimental setup due to continuous monitoring; the light reflection of the objects alongside the edges; and the luminance effect on the objects. The effect of wind on the plant leaves, the darkness or shadow of leaves on each other for one specific plant with multiple leaves, and the effect of shade were also responsible for the imprecise data collection.

Despite these factors, the ROI was kept stationary for both the RFIP and reference data collection. Moreover, the RFIP was placed at the same height as the ground surface for all data collection with the help of a custom-built wooden frame. Overall, the RFIP system showed a great potentiality in the lab, outdoor, and field environment for real-time object and plant detection using single, lightweight, and cost-effective FPGA hardware.

Precise field data collection is the key to support on-the-spot farm management decisions and the developed real-time crop monitoring system proved its proficiency in this regard. This real-time crop monitoring system might be one of the best possible solutions in the current PA market for accessible farm management services.

CHAPTER 6. CONCLUSIONS

After analyzing the existing methods of acquiring agricultural imagery, it was determined that a new strategy and system for real-time crop monitoring using computationally efficient FPGA hardware would provide a powerful solution to solve current demands in PA. Hence, a real-time crop monitoring system that included the RFIP and the RTK-GPS, was developed in this study.

With the intention of responding to the current limitations of high-resolution imagery and the need for a more accurate and precise GPS for real-time crop monitoring PA applications, this study showed great potential for real-world application. Here, a real-time crop monitoring system was developed that included a high resolution, and high-speed image acquisition and image processing units using the same FPGA platform; and an RTK-GPS with 8 cm positional accuracy, to compensate the current PA limitations for on-the-spot farm management solutions.

The proposed system was able to minimize the imaging limitations in digital agriculture related to computational complexity, image resolution, and time of deploying this photographic technology and facilitate real-time, actionable management strategies in the field. To reduce human errors and get more precise real-time data, future research should include the development of an agrobot. The agrobot should integrate the RFIP, the RTK-GPS, and the battery sources. Also, an adjustable shade should be included to reduce luminance effect on the ROI, and a remote-control system to move the system along the crop rows. However, the image sensor should be upgraded with automatic exposure control, global shutter, and polarizing filter attached to the lens. To avoid the pixel noise from the captured images, the development of a single or multiple noise reduction filters will be an ideal solution.

Incorporating all the modifications mentioned above, this proposed real-time crop monitoring system could be deployed on an unmanned ground vehicle. Furthermore, the developed system, with a lightweight FPGA nano board, would also be applicable for integration on an unmanned aerial vehicle.

REFERENCES

- Abbadi, N. E., & Saad, L. A. (2013). Automatic Detection and Recognize Different Shapes in an Image. *International Journal of Computer Science*, 162-166.
- AlAli, M. I., Mhaidat, K. M., & Aljarrah, I. A. (2014). Implementing Image Processing Algorithms on FPGAs. *2013 IEEE Jordan Conference on Applied Electrical Engineering and Computing Technologies (AEECT)* (pp. 118-123). Jordan: IEEE.
- Al-Gaadi, K. A., Hassaballa, A. A., Tola, E., Kayad, A. G., Madugundu, R., Alblewi, B., & Assiri, F. (2016). Prediction of Potato Crop Yield Using Precision Agriculture Techniques. *Public Library of Science One*.
- Asano, S., Maruyama, T., & Yamaguchi, Y. (2009). Performance comparison of FPGA, GPU and CPU in image processing. *2009 International Conference on Field Programmable Logic and Applications*. Prague: IEEE.
- Bannister, R., Gregg, D., Wilson, S., & Nisbet, A. (2005). FPGA implementation of an image segmentation algorithm using logarithmic arithmetic. *48th Midwest Symposium on Circuits and Systems, 2005* (pp. 810-813). Covington: Institute of Electrical and Electronics Engineers.
- Bhakta, I., Phadikar, S., & Majumder, K. (2019). State-of-the-art technologies in precision agriculture: a systematic review. *Science of Food and Agriculture*.
- Blauth, D. A., & Ducati, J. R. (2010). A Web-based system for vineyards management, relating inventory data, vectors and images. *Computers and Electronics in Agriculture*, 182-188.
- Burgos-Artizzu, X. P., Ribeiro, A., Guijarro, M., & Pajares, G. (2011). Real-time image processing for crop/weed discrimination in maize fields. *Computers and Electronics in Agriculture*, 337-346.
- Caballero, D., Calvini, R., & Amigo, J. M. (2020). Chapter 3.3 - Hyperspectral imaging in crop fields: precision agriculture. *Data Handling in Science and Technology*, 453-473.
- Canada, S. (2015, 11 25). *Crop Monitoring & Damage Assessment*. Retrieved from Government of Canada: <https://www.nrcan.gc.ca/earth-sciences/geomatics/satellite-imagery-air-photos/satellite-imagery-products/educational-resources/14652>
- Canada, S. (2017). *Canadian agriculture: evolution and innovation*. Statistics Canada.
- Canada, S. (2017). *Growing opportunity through innovation in agriculture*. Statistics Canada.

- Canada, S. (2018). *Change in total area of land in crops*. Statistics Canada.
- Canada, S. (2018). *Proportion of farms using computers/laptops for farm management*. Statistics Canada.
- Canada, S. (2021). *Employee wages by occupation*. Statistics Canada.
- Chattha, H. S., Zaman, Q. U., Chang, Y. K., Read, S., Schumann, A. W., Brewster, G. R., & Farooque, A. A. (2014). Variable rate spreader for real-time spot-application of granular fertilizer in wild blueberry. *Computers and Electronics in Agriculture*, 70-78.
- Cointault, F., Newspapers, L., Rabatel, G., & Germain, C. (2012). Texture, Color and Frequential Proxy-Detection Image Processing for Crop Characterization in a Context of Precision Agriculture. In *Agricultural Science* (pp. 49-70). France: INTech.
- Das, A. K. (2020, October). Development of an Automated Debris Detection System for Wild Blueberry Harvesters using a Convolutional Neural Network to Improve Food Quality. *Faculty of Graduate Studies Online Theses*. Truro, Nova Scotia, Canada: Dalhousie University.
- Davies, I. J. (2001). Empirical correction factor for the best estimate of Weibull modulus obtained using linear least squares analysis. *Materials Science Letters*, 997-999.
- Dorj, U.-O., Lee, M., & Yun, S.-s. (2017). An yield estimation in citrus orchards via fruit detection and counting using image processing. *Computers and Electronics in Agriculture*, 103-112.
- Dou, R., Liu, L., Liu, J., & Wu, N. (2019). Development of high-speed camera with image quality evaluation. *2019 IEEE 8th Joint International Information Technology and Artificial Intelligence Conference (ITAIC)* (pp. 1404-1408). Chongqing: IEEE.
- El-Medany, W. M., & El-Sabry, M. R. (2008). GSM-based remote sensing and control system using FPGA. *2008 International Conference on Computer and Communication Engineering*. Kuala Lumpur, Malaysia: IEEE.
- Esau, T. J., Zaman, Q. U., Chang, Y. K., Schumann, A. W., Percival, D. C., & Farooque, A. A. (2014). Spot-application of fungicide for wild blueberry using an automated prototype variable rate sprayer. *Precision Agriculture*, 147-161.
- FAO. (2020). *The State of Food Security and Nutririon in the World*. Food and Agriculture Organization of the United Nations.
- FAO. (2021). *Hunger and food insecurity*. Food and Agriculture Organization of the United Nations.

- FAO. (2021). *Integrated Weed Management*. Food and Agriculture Organizations of the United Nations.
- FAO. (2021). *Sustainable Crop Production Intensification*. Food and Agriculture Organization of the United Nations.
- Gonzalez, C., Mozos, D., Resano, J., & Plaza, A. (2011). FPGA Implementation of the N-FINDR Algorithm for Remotely Sensed Hyperspectral Image Analysis. *IEEE Transactions on Geoscience and Remote Sensing*, 374 - 388.
- González, C., Sánchez, S., Paz, A., Resano, J., Mozos, D., & Plaza, A. (2013). Use of FPGA or GPU-based architectures for remotely sensed hyperspectral image processing. *Integration*, 89-103.
- Guo, T., Kujirai, T., & Watanabe, T. (2012). Mapping Crop Status from AN Unmanned Aerial Vehicle for Precision Agriculture Applications. *ISPRS International Archives of the Photogrammetry, Remote Sensing and Spatial Information Sciences* (pp. 485-490). Melbourne: ISPRS Congress.
- Gutiérrez, F., Htun, N. N., Schlenz, F., Kasimati, A., & Verbert, K. (2019). A review of visualisations in agricultural decision support systems: An HCI perspective. *Computers and Electronics in Agriculture*, 1-28.
- Johnston, C. T., Gribbon, K. T., & Bailey, D. G. (2004). Implementing Image Processing Algorithms on FPGAs. *Proceedings of the Eleventh Electronics New Zealand Conference, ENZCon'04* (pp. 118-123). Palmerston North: Cite Seer.
- Kestur, S., Davis, J. D., & Williams, O. (2010). BLAS Comparison on FPGA, CPU and GPU. *IEEE Computer Society Annual Symposium on VLSI*. Lixouri, Greece: IEEE.
- Lamb, D. W., & Brown, R. B. (2001). PA—Precision Agriculture: Remote-Sensing and Mapping of Weeds in Crops. *Journal of Agricultural Engineering Research*, 117-125.
- Lin, L. I.-K. (1992). Assay Validation Using the Concordance Correlation Coefficient. *Biometrics*, 599-604.
- Ling, G., & Bextine, B. (2017, June 26). *Precision Farming Increases Crop Yields*. Retrieved from Scientific American: <https://www.scientificamerican.com/article/precision-farming/>
- Lorite, I. J., García-Vila, M., Santos, C., Ruiz-Ramos, M., & Fereres, E. (2013). AquaData and AquaGIS: Two computer utilities for temporal and spatial simulations of water-limited yield with AquaCrop. *Computers and Electronics in Agriculture*, 227-237.

- MacLean, W. J. (2005). An Evaluation of the Suitability of FPGAs for Embedded Vision Systems. *2005 IEEE Computer Society Conference on Computer Vision and Pattern Recognition (CVPR'05) - Workshops*. San Diego: Institute of Electrical and Electronics Engineers.
- Moshnyaga, V. G., Hasimoto, K., & Suetsugu, T. (2008). FPGA design for user's presence detection. *2008 15th IEEE International Conference on Electronics, Circuits and Systems* (pp. 1316-1319). Malta: IEEE.
- Mulla, D. J. (2013). Twenty five years of remote sensing in precision agriculture: Key advances and remaining knowledge gaps. *Biosystems Engineering*, 358-371.
- Myers, S. (2020, October 12). *6 ways data analytics leads to better decisions for farmers*. Retrieved from Sas Blogs: <https://blogs.sas.com/content/sascom/2020/10/12/6-ways-data-analytics-leads-to-better-decisions-for-farmers/>
- Ogier, A., Dorval, T., & Genovesio, A. (2007). Biased Image Correction Based on Empirical Mode Decomposition. *2007 IEEE International Conference on Image Processing*. San Antonio, TX, USA: IEEE.
- Price, A., Pyke, J., Ashiri, D., & Cornall, T. (2006). Real Time Object Detection for an Unmanned Aerial Vehicle using an FPGA based Vision System. *Proceedings 2006 IEEE International Conference on Robotics and Automation* (pp. 2854-2859). Orlando: Institute of Electrical and Electronics Engineers.
- Ramirez-Cortes, J. M., Gomez-Gil, P., Alarcon-Aquino, V., Martinez-Carballido, J., & Morales-Flores, E. (2013, January 18). FPGA-based educational platform for real-time image processing experiments. *Wiley Online Library*, pp. 193-201.
- Rehman, T. U., Zaman, Q. U., Chang, Y. K., Schumann, A. W., Corscadden, K. W., & Esau, T. J. (2018). Optimising the parameters influencing. *Biosystems Engineering*, 85-95.
- Rehman, T. U., Zaman, Q. U., Chang, Y. K., Schumann, A. W., Corscadden, K. W., & Esau, T. J. (2018). Optimising the parameters influencing performance and weed (goldenrod) identification accuracy of colour co-occurrence matrices. *Biosystems Engineering*, 85-95.
- Ruß, G., & Brenning, A. (2010). Data Mining in Precision Agriculture: Management of Spatial Information. *International Conference on Information Processing and Management of Uncertainty in Knowledge-Based Systems* (pp. 350-359). Verlag Berlin Heidelberg: Springer.

- Saddik, A., Latif, R., & Ouardi, A. E. (2021). Low-Power FPGA Architecture Based Monitoring Applications in Precision Agriculture. *Journal of Low Power Electronics and Applications*, 1-17.
- Saddik, A., Latif, R., Elhoseny, M., & Ouard, A. E. (2021). Real-time evaluation of different indexes in precision agriculture using a heterogeneous embedded system. *Sustainable Computing: Informatics and Systems*.
- Saegusa, T., Maruyama, T., & Yamaguci, Y. (2008). How fast is an FPGA in image processing? *2008 International Conference on Field Programmable Logic and Applications*. Heidelberg: IEEE.
- Salazar, S. (2015, August 17). *Google Maps Platform*. Retrieved from Maps data and Google Maps APIs enable a new approach to agriculture: <https://mapsplatform.googleblog.com/2015/08/maps-data-and-google-maps-apis-enable.html>
- Sawant, S., Durbha, S. S., Jagarlapudi, & Adinarayana. (2017). Interoperable agro-meteorological observation and analysis platform for precision agriculture: A case study in citrus crop water requirement estimation. *Computers and Electronics in Agriculture*, 175-187.
- Saxena, L., & Armstrong, L. (2014). A survey of image processing techniques for agriculture. *Asian Federation for Information Technology in Agriculture* (pp. 401-413). Edith Cowan University Research Online.
- Sayer, A. M., Govaerts, Y., Kolmonen, P., Luffarelli, M., Mielonen, T., Patadia, F., . . . Witek, M. L. (2020). A review and framework for the evaluation of pixel-level uncertainty estimates in satellite aerosol remote sensing. *Atmospheric Measurement Techniques*, 373-404.
- Schellberg, J., Hill, M. J., Gerhards, R., Rothmund, M., & Braun, M. (2008). Precision agriculture on grassland: Applications, perspectives and constraints. *European Journal of Agronomy*, 59-71.
- Shin, J., Chang, Y. K., Heung, B., Nguyen-Quang, T., Price, G. W., & Al-Mallahi, A. (2020). Effect of directional augmentation using supervised machine learning technologies: A case study of strawberry powdery mildew detection. *Biosystems Engineering*, 49-60.
- Silvan-Cardenas, J. L., & Wang, L. (2008). Sub-pixel confusion–uncertainty matrix for assessing soft classifications. *Remote Sensing of Environment*, 1081-1095.

- Sood, K., Singh, S., Rana, R. S., Rana, A., Kalia, V., & Kaushal, A. (2015). Application of GIS in precision agriculture. *National Seminar on "Precision Farming technologies for high Himalayas"*. Ladakh: ResearchGate.
- Sun, H., Slaughter, D. C., Ruiz, M. P., Gliever, C. J., Upadhyaya, S. K., & Smith, R. F. (2010). RTK GPS mapping of transplanted row crops. *Computers and Electronics in Agriculture*, 32-37.
- Teillet, P. M. (2007). Image correction for radiometric effects in remote sensing. *International Journal of Remote Sensing*, 1637-1651.
- Tlelo-Cuautle, E., Carbajal-Gomez, V. H., Obes, P. J., Rangel-Magdaleno, J. J., & Núñez-Pérez, J. C. (2015). FPGA realization of a chaotic communication system applied to image processing. *Nonlinear Dynamics*, 1879-1892.
- Triantafyllou, A., Sarigiannidis, P., & Bibi, S. (2019). Precision Agriculture: A Remote Sensing Monitoring System Architecture. *Information*.
- Trimberger, S. M. (1994). *Field-Programmable Gate Array Technology*. New York: Kluwer Academic Publisher.
- Tsouros, D. C., Bibi, S., & Sarigiannidis, P. G. (2019, November 11). A Review on UAV-Based Applications for Precision Agriculture. *IoT Applications and Industry 4.0*, 1-26.
- Valle, S. S. (2020). *Agriculture 4.0*. Rome: Food and Agriculture Organization of the United Nations.
- Vibhute, A., & Bodhe, S. K. (2012). Applications of Image Processing in Agriculture: A Survey. *International Journal of Computer Applications*, 0975-8887.
- Wachowiak, M. P., Waltersb, D. F., Kovacs, J. M., Wachowiak-Smolíková, R., & James, A. L. (2017). Visual analytics and remote sensing imagery to support community-based research for precision agriculture in emerging areas. *Computers and Electronics in Agriculture*, 149-164.
- Worldbank. (2019, November 30). *Employment in agriculture (% of total employment) (modeled ILO estimate)*. Retrieved from World Bank Group: <https://data.worldbank.org/indicator/SL.AGR.EMPL.ZS?end=2019&start=1991&view=chart>
- Worldmeters. (2019, November 30). *World Population: Past, Present, and Future*. Retrieved from Worldmeters: <https://www.worldometers.info/world-population/#growthrate>

- Zhai, X., Bensaali, F., & Ramalingam, S. (2011). Real-time license plate localisation on FPGA. *CVPR 2011 WORKSHOPS* (pp. 14-19). Colorado: Institute of Electrical and Electronics Engineers.
- Zhang, N., Wang, M., & Wang, N. (2002). Precision agriculture—a worldwide overview. *Computers and Electronics in Agriculture*, 113-132.
- Zhang, Q. (2016). *Precision Agriculture Technology for Crop Farming*. The Hague: Taylor & Francis.
- Zude-Sasse, M., Fountas, S., Gemtos, T. A., & Abu-Khalaf, N. (2016). Applications of precision agriculture in horticultural crops. *European Journal of Horticultural Science (eJHS)*, 78-90.

APPENDIX. RAW DATA

1. RAW Pixel Data from Lab Evaluation

Algorithms	Objects	RFIP Area	DSLR Area
R	1	135367	130390
R	1	135279	130524
R	1	135424	130521
R	1	133683	131077
R	1	133581	130390
R	1	133675	129838
R	1	133537	129887
R	1	133721	129413
R	1	133565	129094
R	1	133685	130230
R	2	96707	89900
R	2	96747	89611
R	2	96806	89580
R	2	95540	89851
R	2	95660	89809
R	2	95576	90258
R	2	95604	89893
R	2	95557	89821
R	2	95649	90951
R	2	95607	90532
R	3	84448	76894
R	3	84402	77267
R	3	84438	76504
R	3	82913	76761
R	3	82943	76761
R	3	82909	76745
R	3	82957	76352
R	3	82929	76708
R	3	82933	76668
R	3	82920	76707
R	4	85237	77936
R	4	85221	77859
R	4	85295	77278
R	4	84894	77486
R	4	85043	77500
R	4	84953	77871
R	4	85058	77935
R	4	84895	77433
R	4	84966	77634
R	4	84928	77869

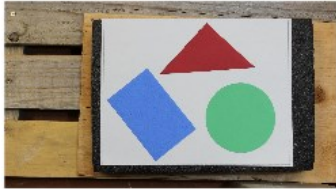
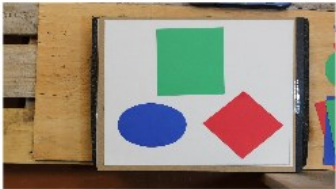
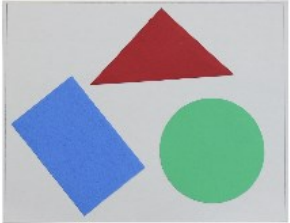
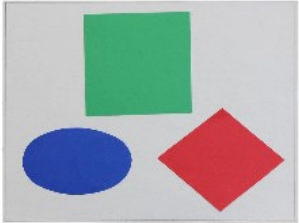
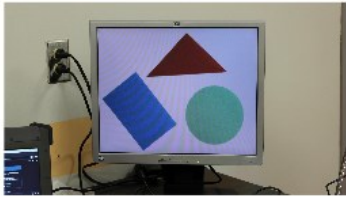
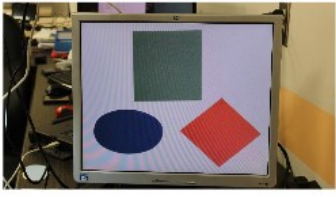

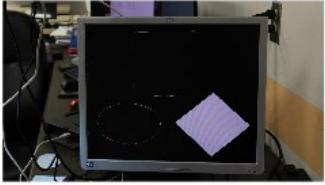



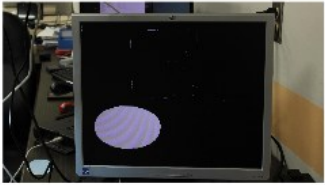
R	5	87381	80799
R	5	87291	80112
R	5	87378	80325
R	5	88532	80295
R	5	88405	80938
R	5	88476	80669
R	5	88448	80681
R	5	88552	79957
R	5	88433	80694
R	5	88455	80443
R	6	57060	49491
R	6	57056	50322
R	6	57078	49423
R	6	58839	50075
R	6	58789	49463
R	6	58844	49418
R	6	58801	49088
R	6	58798	49296
R	6	58842	49070
R	6	58804	49760
R	7	51129	43322
R	7	51055	43238
R	7	51141	43238
R	7	53161	43310
R	7	52964	43107
R	7	53047	43126
R	7	53029	43265
R	7	53049	43261
R	7	53014	43357
R	7	53050	44211
R	8	178300	174017
R	8	178383	173864
R	8	178331	173424
R	8	177322	173489
R	8	177462	173510
R	8	177407	172643
R	8	177514	172774
R	8	177321	172424
R	8	177487	173664
R	8	177323	172465
R	9	32631	23425
R	9	32591	23330
R	9	32638	23567
R	9	34000	23505
R	9	34003	23853
R	9	33998	23626

R	9	33978	23388
R	9	34018	23403
R	9	33965	23408
R	9	34002	23549
R	10	40515	29894
R	10	40567	29469
R	10	40575	29430
R	10	43037	29285
R	10	43112	29814
R	10	43046	29497
R	10	43096	29172
R	10	43075	29213
R	10	43108	28979
R	10	43051	29241
R	11	33987	24429
R	11	34045	24418
R	11	34028	24495
R	11	38180	24581
R	11	38082	24511
R	11	38152	24602
R	11	38091	25905
R	11	38148	25348
R	11	38116	25676
R	11	38131	25907
R	12	85915	77314
R	12	85814	76625
R	12	85915	76297
R	12	88086	77562
R	12	88204	77233
R	12	88196	77491
R	12	88178	77204
R	12	88170	77035
R	12	88205	77740
R	12	88194	76577
R	13	89515	80385
R	13	89386	80037
R	13	89472	80273
R	13	90561	80237
R	13	90476	79838
R	13	90627	80740
R	13	90493	79702
R	13	90584	80737
R	13	90479	80161
R	13	90489	80339
R	14	59376	49555
R	14	59293	49301

R	14	59369	49133
R	14	60854	49016
R	14	60942	48923
R	14	60872	49379
R	14	60942	49404
R	14	60864	49294
R	14	60941	49244
R	14	60863	49304
R	15	53339	43278
R	15	53338	43017
R	15	53292	43263
R	15	53896	43290
R	15	53813	43520
R	15	53922	43804
R	15	53914	43342
R	15	53893	42901
R	15	53872	43288
R	15	53862	43330
R	16	60781	49621
R	16	60822	49299
R	16	60773	49139
R	16	60637	49670
R	16	60700	49328
R	16	60619	49409
R	16	60683	49614
R	16	60621	49384
R	16	60717	49702
R	16	60621	48972
G	1	129263	129470
G	1	129169	129160
G	1	129233	128822
G	1	129517	129436
G	1	129409	129112
G	1	129440	129289
G	1	129376	128928
G	1	129514	128665
G	1	129413	128066
G	1	129419	128889
G	2	91544	89601
G	2	91443	90039
G	2	91519	90621
G	2	91168	89248
G	2	91138	89403
G	2	91194	89717
G	2	91119	89311
G	2	91165	90106

G	2	91032	89424
G	2	91187	89837
G	3	78562	76104
G	3	78616	76332
G	3	78596	76376
G	3	78563	76354
G	3	78479	75839
G	3	78613	76395
G	3	78528	76061
G	3	78588	76328
G	3	78466	76403
G	3	78643	76239
G	4	80221	77384
G	4	80104	77369
G	4	80213	77934
G	4	79901	77838
G	4	80071	77794
G	4	79990	77542
G	4	80064	77424
G	4	79892	76489
G	4	80053	77638
G	4	79986	76606
G	5	84021	80807
G	5	83865	80733
G	5	83988	80361
G	5	83494	80611
G	5	83384	80541
G	5	83469	80767
G	5	83397	80604
G	5	83603	80920
G	5	83346	80320
G	5	83472	80320
G	6	54160	49987
G	6	54067	50161
G	6	54104	50464
G	6	54060	50012
G	6	53929	50063
G	6	54063	50247
G	6	53933	50248
G	6	54027	50149
G	6	53961	50205
G	6	54035	50144

2. Example of RAW Image Data from Lab Evaluation

<p>DSLR Captured Images of Objects</p>		
<p>Processed DSLR Captured Images of Objects</p>		
<p>RFIP Captured Images of Objects</p>		
<p>RFIP Detected Images of Objects using R-ratio Algorithm</p>		
<p>RFIP Detected Images of Objects using G-ratio Algorithm</p>		
<p>RFIP Detected Images of Objects using B-ratio Algorithm</p>		

3. RAW Pixel Data from Outdoor Evaluation

Plant Samples	RFIP Area	Web Camera Area
1	42391	46654
2	42446	47403
3	42792	47163
4	42529	47307
5	42587	47699
6	42890	47687
7	42935	47126
8	42890	48000
9	42931	47684
10	42834	48137
11	49334	55154
12	49037	55003
13	49072	55384
14	48961	55308
15	49198	55000
16	49095	54894
17	49380	55255
18	49426	55193
19	49030	55119
20	49127	55291
21	78125	87068
22	78124	87691
23	77595	87582
24	77957	87372
25	77994	87356
26	77919	88301
27	77767	87250
28	78015	86943
29	77947	89390
30	77547	88830
31	56139	58944
32	56285	58617
33	56313	59358
34	56251	59195
35	56350	58833
36	55725	59220
37	56007	59322
38	56201	58790
39	56246	58962
40	56176	59244
41	59577	66416
42	59544	66382
43	59554	66598













44	59505	66518
45	59450	66403
46	59042	66772
47	59150	66651
48	59119	66697
49	59240	66562
50	58913	66571
51	103641	123088
52	104173	123440
53	103617	123244
54	103660	122598
55	104122	123459
56	104121	123571
57	103562	122915
58	103888	121768
59	103593	123285
60	103348	123598
61	62641	69642
62	62643	69912
63	62673	69834
64	62634	69862
65	62668	69997
66	62293	70006
67	62593	69742
68	62590	69172
69	62640	69657
70	62639	69529
71	55027	62534
72	55102	62213
73	54859	62306
74	54880	62419
75	55241	62469
76	55234	62509
77	55254	62545
78	55332	62375
79	55314	62668
80	54904	62583
81	111565	125668
82	111274	126489
83	111385	125884
84	111615	126153
85	111693	125778
86	111661	126026
87	111962	124901
88	112053	126065
89	111824	125961

90	112185	125639
91	54093	59823
92	54089	59973
93	53990	59946
94	53904	59708
95	53777	59776
96	54123	59741
97	54187	59646
98	54229	60104
99	54217	60164
100	54328	60159
101	109075	125539
102	108703	124637
103	108992	124921
104	108942	125560
105	109447	124784
106	109409	124229
107	109383	124163
108	109262	124031
109	109037	124636
110	109398	124647
111	75706	84944
112	75372	85314
113	75452	84908
114	75004	84705
115	75070	85390
116	75561	84628
117	75242	85050
118	74833	84733
119	75179	84223
120	75391	84496
121	55133	61399
122	55072	61219
123	54656	60904
124	54688	61416
125	55118	60959
126	54997	60680
127	54879	61599
128	55068	61288
129	55192	61215
130	54945	61457
131	73434	81322
132	73438	82017
133	73369	82353
134	73742	82070
135	73513	81653

136	73261	81929
137	73206	81472
138	74290	81914
139	73375	81808
140	73488	82029
141	52107	57065
142	52180	56633
143	52179	56626
144	52210	56413
145	52018	56781
146	52077	56568
147	52225	56430
148	52355	57012
149	52392	56950
150	52379	56940
151	50981	58200
152	51048	58042
153	51260	58489
154	51441	57767
155	51466	58169
156	51463	58383
157	51515	58559
158	51031	58382
159	51295	58263
160	51076	57894
161	75428	82821
162	75186	82287
163	74790	82520
164	75132	82155
165	74982	82829
166	74841	83020
167	74762	82609
168	74701	82286
169	75161	81967
170	75174	81988
171	75537	85055
172	75165	84455
173	75558	83902
174	75428	84224
175	75841	83962
176	75664	84157
177	75473	83765
178	75231	83798
179	75335	83459
180	75675	83600
181	78828	89664

182	78774	89253
183	78599	89890
184	78710	89551
185	78554	89072
186	79012	89295
187	78951	89133
188	79027	88870
189	78350	88839
190	78700	89670
191	73896	85161
192	73936	84930
193	73763	84968
194	73524	84871
195	73568	84294
196	73956	84790
197	74012	84842
198	73698	84414
199	73418	84805
200	73455	84628
201	92286	102879
202	91998	102649
203	92050	103175
204	91766	102558
205	91862	102483
206	91846	102602
207	92335	102579
208	92288	102658
209	91807	102808
210	91639	102201
211	51290	56775
212	51330	57236
213	51207	56929
214	51699	56744
215	51802	56901
216	51680	56763
217	51747	57082
218	51818	56791
219	51590	56941
220	51745	57246

4. Example of RAW Image Data from Outdoor Evaluation

<p>Plant Samples</p>		
<p>Web Camera Captured Images of Plants</p>		
<p>Processed Web Camera Captured Images of Plants</p>		
<p>Processed Binary Web Camera Captured Images of Plants using G-ratio Algorithm</p>		
<p>RFIP Captured Images of Plants</p>		
<p>RFIP Detected Images of Plants using G-ratio Algorithm</p>		

5. RAW Pixel Data from Field Evaluation







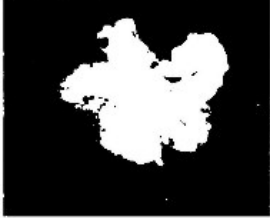



Plant Samples	RFIP Area	Web Camera Area
1	50597	105605
2	56424	112878
3	56908	116785
4	56831	113262
5	57096	111373
6	56982	112490
7	56566	113022
8	95859	148470
9	95146	150293
10	93301	146447
11	94841	151527
12	94302	152271
13	95249	151712
14	95256	151108
15	108576	162412
16	109517	170544
17	111499	170211
18	112136	171710
19	112654	169813
20	112260	169332
21	111665	166651
22	59876	97063
23	60022	96854
24	60340	101450
25	60929	106505
26	59951	96268
27	60272	98987
28	59664	97295
29	163829	217826
30	161299	209755
31	162524	214002
32	162250	208905
33	162393	211373
34	162148	205108
35	162599	216317
36	100205	162880
37	102514	170594
38	102883	168981
39	103509	171028
40	104292	177802
41	100064	166179
42	95703	163669
43	53667	98706

44	53512	99697
45	53117	103580
46	52924	105015
47	52517	104450
48	52327	103290
49	53859	99330
50	87907	149662
51	87693	150055
52	87639	150664
53	88138	148784
54	87728	146208
55	87865	145735
56	86462	143844
57	54822	123113
58	53159	107944
59	52559	107909
60	52468	104682
61	52702	109359
62	51856	102987
63	52456	109863
64	36949	96891
65	35450	97726
66	35102	97524
67	35007	94743
68	34877	91517
69	34557	93439
70	34974	97126
71	63265	114112
72	63603	116415
73	63460	115435
74	63770	116043
75	63718	111243
76	63086	115523
77	63807	116706
78	144215	242515
79	142234	239223
80	143889	239851
81	144790	239651
82	145062	238725
83	145230	238635
84	146279	240750
85	38967	108616
86	38691	110705
87	38788	109505
88	38550	110652
89	38912	108716

90	38616	112454
91	38768	109197
92	88639	179499
93	87130	176008
94	87554	175875
95	87387	175930
96	88018	174577
97	86896	172592
98	86790	174644
99	69258	135094
100	68603	133094
101	68094	131715
102	67870	131489
103	67727	132659
104	67349	135322
105	66176	137809
106	44255	111478
107	43830	111720
108	43763	113473
109	43913	106295
110	43791	116860
111	43878	113548
112	43836	115167
113	46220	114831
114	45349	120675
115	43591	116181
116	42879	118783
117	43510	119111
118	41842	112654
119	40768	114872
120	16267	114273
121	24063	111168
122	31189	116423
123	30069	114766
124	30199	121966
125	29537	118136
126	29725	117313
127	92972	146026
128	93000	147284
129	93827	148430
130	93816	149275
131	93593	151295
132	93739	151926
133	93909	151420
134	80747	112598
135	80268	112451

136	80101	115374
137	80098	115814
138	80077	116548
139	80069	116777
140	80108	115524
141	127102	189921
142	127636	187506
143	127454	190112
144	127106	189068
145	127257	189231
146	127229	189194
147	127140	188432

6. Example of RAW Image Data from Field Evaluation

<p>Plant Samples</p>		
<p>Web Camera Captured Images of Plants</p>		
<p>Processed Web Camera Captured Images of Plants</p>		
<p>Processed Binary Web Camera Captured Images of Plants using G-ratio Algorithm</p>		
<p>RFIP Captured Images of Plants</p>		
<p>RFIP Detected Images of Plants using G-ratio Algorithm</p>	